RESEARCH IN ATMOSPHERIC RADIATION

A Report of Research Conducted in
the Department of Meteorology,
The University of Wisconsin

Annual Report on WBG-88
1966-67

The Research reported in this
document was funded by the
Institutes for Environmental
Research, Environmental
Science Services Administration,
Boulder, Colorado

March, 1968

ACKNOWLEDGMENTS

We wish to express our gratitude to the Institutes for Environmental Research for providing the funding for the research reported herein and for allowing this research to proceed in an unrestricted and productive manner.

Many persons have contributed to the research and preparation of this document. Our thanks to Mrs. Lois Stearns, Mr. John Stremikis and Mr. Terry Yonker for their roles in the reduction of the radiation sonde ascents. We express our gratitude to Miss Betty Erwin for the typing and preparation of this manuscript.

TABLE OF CONTENTS

A Radiation Model in Which The Effects of Clouds are Simulated From Moisture and Temperature Parameters

STEPHEN K. COX

University of Wisconsin
Madison, Wisconsin

TABLE OF CONTENTS

ABSTRACT

This thesis describes a means to include the effects of clouds on solar and longwave radiation transfer in a primitive equation numerical general circulation model where moisture is carried as a dependent variable. Specific information on cloudiness is not required even though the radiation results include the likely effects of clouds. Vertical profiles of moisture and temperature are used as input data, and the radiative effects of clouds are inferred from the profiles. The infrared technique was developed from a large number of radiation sonde observations representing various locations, seasons and sky conditions.

The infrared computation was made for two sets of independent observations of pressure, temperature and moisture, for which coincident radiation measurements were available. A comparison between observed and calculated radiative cooling rates showed that the technique can reproduce synoptic-scale radiative cooling patterns. The root mean square deviations between observed and calculated daily cooling rates were 34% and 26% of the observed mean cooling rates for the tropics and middle latitudes, respectively.

Because the errors in estimates for the midlatitude test sample were normally distributed, the error for the whole globe or for several days is likely to be much smaller. An individual error of up to 30% in the application to a numerical general circulation model

is not serious because the model acts as a smoothing filter. The data sample in the tropics was much more limited, and the errors departed from a normal distribution in a manner which will introduce a slight bias. As more tropical data becomes available it will be necessary to further test and develop the infrared technique.

A technique to calculate solar warming, based on the method of Hanson, et al. (1967), is shown. The method takes the effects of clouds into account without relying on specific cloud information. The solar method has not been tested. Initial calculations suggest the technique may yield anomalously high solar absorption in tropical latitudes.

LIST OF SYMBOLS

γ	Temperature lapse rate
λ	Moisture power law exponent
θ_d	Rossby potential temperature
$\theta(t)$	Zenith angle of sun at time, t
ρ	Density of dry air
$\tilde{\tau}$	Grey, layer transmissivity
A	Coefficient in regression equation
B	Black body irradiance
C_p	Specific heat of dry air
D	Coefficient in empirical solar absorption distribution function
e	Base of natural logarithms
E	Absorbed solar energy
g	Gravitational acceleration
K	Effective absorption coefficient as used in exponential function representing transmissivity
p	Pressure
PMSL	Mean sea level pressure
q_a	Fractional shortwave absorption
q'_a	Fractional shortwave absorption for the surface to 200 mb layer
R^+ ,R^-	Upward and downward infrared irradiances, respectively
R_n	Net infrared irradiance, $R_n = R^+ - R^-$

S	Solar constant
T	Absolute temperature of air
T_i	Temperature at top of inversion
t	Time
u	Optical mass of water vapor
u^*	Optical path, $u^* = u \sec \theta$
w	Mixing ratio of water vapor
X	Parameter in regression equation
z	Vertical coordinate in x, y, z system

Notation

o	Refers to reference level
A(X-Y)	Parameter A applies to the layer Xmb to Y mb

Introduction

The purpose of this research is to develop empirical radiation formulas, based on actual measurements of radiative cooling and warming, for use in a numerical model of the general circulation.

The simplest numerical model, the barotropic model, rearranges the kinetic energy of the initial state of a dry atmosphere. Since there are no energy sources or sinks, no radiation effects are considered. The adiabatic baroclinic numerical model allows for conversion between available potential energy and kinetic energy, but like the barotropic case, does not allow for any diabatic sources or sinks of energy.

The "primitive equation" numerical model includes the thermodynamic equation, and thus sources and sinks of heat energy. The primary source of energy for driving the atmosphere is the sun, and solar energy is entered into the model as a function of latitude. Clearly, in order to balance the incoming solar energy, a radiative loss from the earth's surface and atmosphere is required to act as a heat sink.

The atmosphere must be "wet" enough to have an appropriate emissivity in order to radiate realistically. However, only the most sophisticated general circulation models include moisture as a variable. Only in these can time variation of radiation cooling be realized.

1. Radiation in the Atmosphere

The infrared cooling of the atmosphere is governed by its optically active gaseous constituents and the liquids and solids suspended in it. The radiative consequences of clouds are so large that they tend to mask the effects of the gaseous constituents. For this reason, when computing radiative cooling, it is extremely important to know whether or not clouds are present and to consider the cloud height, thickness and emissivity. Neglect of cloud features would lead to large errors in infrared cooling estimates.

The gases of prime importance in the radiative budget of the troposphere are water vapor and carbon dioxide. Brooks (1950) estimates that in the lower troposphere the infrared cooling affected by carbon dioxide is about 3% that due to water vapor. In the upper troposphere under clear conditions the radiation divergence due to carbon dioxide and water vapor are of the same order of magnitude. However, in the presence of clouds, radiative divergence due to water substance is dominant. Ozone, while playing an important radiative role in the stratosphere, is relatively unimportant in the troposphere.

Since clouds have a dominant effect, we cannot ignore them when computing radiative cooling. However, the numerical modeler has no explicit information on cloud structure or characteristics. The only information available are the temperature profile and, in some cases, the moisture profile. We must ask, is it possible to use the temperature and water vapor distributions as indicators of the radiative effects of clouds?

Manabe, et al. (1965) have used a similar technique in a nine-level model in which they treat rainfall but not clouds. They found

that in order to have realistic rainfall, it was necessary to let condensation occur when the relative humidity was less than 100%. This is not too surprising, although most clouds have a relative humidity near 100%, since the volume represented by a grid point of a typical mesh size is not completely filled with clouds. Apparently when the volume-mean relative humidity is about 70%, parts of the volume are wet enough to rain. We will treat certain questions of radiative cooling in a similar manner.

Up to the present time, numerical general circulation models have relied upon theoretical computations of radiative cooling based upon climatological water vapor and cloud data. Such a treatment satisfies the radiative boundary requirement that the longwave loss in the general circulation model must balance the shortwave energy absorbed by the system. If we want synoptic features to be, in part, a result of the radiative cooling field, climatological data cannot furnish adequate detail of the radiative cooling field. According to Suomi and Shen (1963) infrared cooling may have a significant effect on synoptic scale circulations. Dutton and Johnson (1967) show that radiative cooling, while substracting heat from a system, actually generates available potential energy.

2. The Cloud Problem

Let us explore the extent to which information on clouds is available from the moisture and temperature profiles. The cloud information needed for radiative computations includes:

1. Cloud coverage
2. Cloud height
3. Cloud thickness
4. Cloud emissivity

Radiosonde measurements of temperature and moisture are commonly used to detect cloud presence. This technique is based upon the fact that in a cloud the air should be nearly saturated with water vapor. However, trying to specify cloud coverage by an individual measurement is difficult since a radiosonde may ascend either through the only cloud within many kilometers or through a small hole in an otherwise overcast layer. In either case the moisture measurement may be representative of only a very small volume.

A radiation sonde, used as a cloud detector, does have the advantage that it receives information from a much larger volume than does a moisture or temperature sensor. When the radiation sonde is immersed in a cloud, its indication corresponds to that of the hygristor. However, when the radiometer is above or below a cloud, the radiation to which it responds is a volume integrated signal containing effects of clouds and thus implicitly yielding information on cloud coverage.

Seventy-five percent of the radiant energy incident on the radiometer in an isotropic atmosphere comes from a solid angle of 60° centered on the zenith. At 9.1 km elevation this corresponds to an

area on the earth's surface of 195 sq km. Figure 1 illustrates the volume from which 75% of the upward irradiance at 300 mb originates in an isotropic atmosphere. Thus radiation sonde measurements provide some, although limited, information on cloud cover.

In the multiple regression analysis explained later, coincident measurements of temperature, moisture and radiation parameters were examined to find whatever information on clouds exists in the temperature and moisture profiles. Since the temperature and moisture profiles determine the static stability of the atmosphere, it is plausible to relate the tendency for cloud formation and the potential cloud height and thickness to moisture and temperature.

The cloud thickness, height and emissivity are interrelated parameters. In general, the thicker and lower the cloud, the higher its emissivity. Kuhn (1964) has derived characteristic infrared emissivity ranges which are summarized below.

	Stratus	Alto Stratus	Cirrus
Overcast	1.0	.90	.65
Broken	.75	.45	.20
Scattered	.45	.25	.05

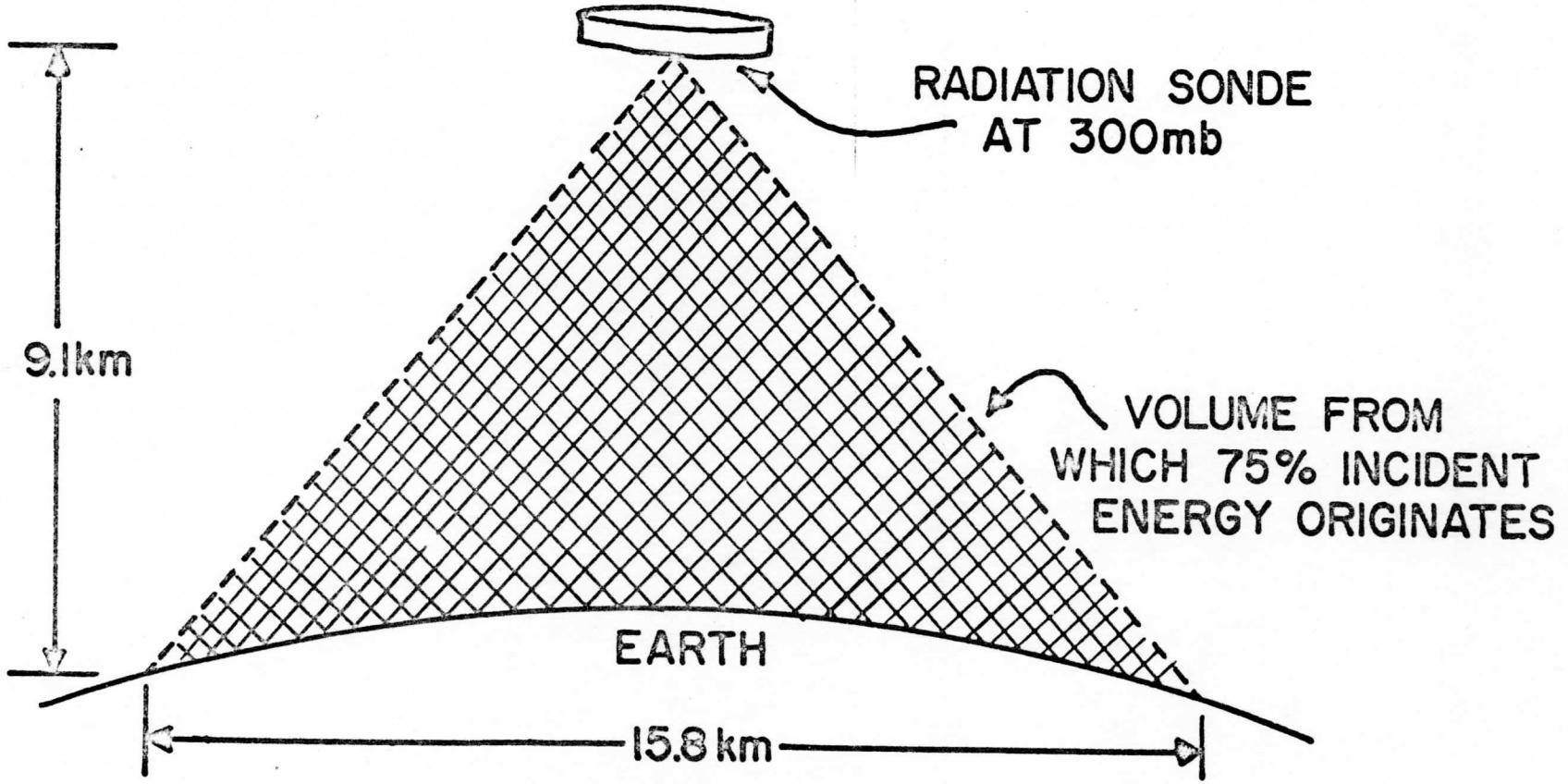

FIGURE 1: Volume from which 75% of upward irradiance at 300 mb originates.

Since the amount of water vapor and the phase of particulate water substance depend on temperature, the cloud height-emissivity relation reported by Kuhn may be due to varying amounts of optically active constituents. High, cold clouds would have smaller optical masses than lower, warmer clouds; therefore, the higher clouds would have lower emissivities.

It is our aim to minimize the number of independent variables required in a computation of radiative cooling. While we could conceivably carry along in a numerical model a detailed table of pressure, temperature and moisture for each grid point, such a procedure would exceed both computer storage and speed limitations. We therefore utilize only four parameters to represent the temperature and moisture profiles. The temperature profile is given by a mean linear lapse rate, γ , and the surface temperature, T_o. For the moisture profile we utilize a power law representation where W_o, the surface mixing ratio, and λ , a numerical parameter representing the vertical gradient of moisture, are sufficient to specify the profile; see equation (3).

Assume λ to be a function of cloudiness. Low values of λ represent sizeable amounts of moisture aloft whereas high values of λ represent smaller amounts of moisture aloft. Thus, one expects clouds to be associated with low values of λ and clearer conditions to be represented by higher values of λ . Table I shows average values of the parameters $\lambda(\text{SFC-600})$, $\lambda(600\text{-}200)$, W_o, W_{600}, W_{200} for one hundred radiation sonde ascents. These ascents were classified as "cloudy" or "cloudless" on the basis of the divergence of the observed equivalent irradiance in comparison with the divergence of

SKY CONDITION	λ	W_o	W_{600}	W_{200}
		SFC - 600 mb layer		
CLOUDY	1.36	5.84	3.22	
CLOUDLESS	4.10	5.83	1.17	
		600 - 200 mb layer		
CLOUDY	4.01		2.01	.014
CLOUDLESS	4.91		1.58	.005
		SFC - 200 mb layer		
CLOUDY	2.18	6.14	2.05	.120
CLOUDLESS	4.23	5.85	.67	.006

TABLE 1. Relationship between sky condition and moisture parameters.

equivalent irradiance computed in a saturated water vapor layer. The table shows that low values of λ correspond to the cloudy cases whereas high values correspond to cloudless situations.

A numerical model, which does not use real data, is not subject to instrumental deficiencies. These deficiencies include everything from instrument failure to inherent limitations of the sensors. One of the most apparent differences between the numerical model data and real data occurs in the moisture profile. Conventional hygristors used on radiosondes are not reliable at temperatures lower than $-40^{o}C$. It is therefore necessary to "fill in" the water vapor profiles with realistic data for the high troposphere. In agreement with Mastenbrook (1966), a mixing ratio of .02 g kg^{-1} was assigned to the 200 mb level. Missing data between the highest non-zero mixing ratio and 200 mb were linearly interpolated with respect to pressure. For the layer from 200 mb to the top of the atmosphere, we assumed a constant optical mass of water vapor of .0015 gm cm^{-2}. Since a calculation of downward irradiance requires a temperature profile to the top of the atmosphere, we assumed a temperature profile above terminal balloon altitude given by Murgatroyd (1957).

3. Infrared Model

3.1 Method

To derive an equation which allows us to infer radiative effects of clouds from temperature and moisture profiles, we define

$$\gamma = -\frac{\partial T}{\partial Z} \tag{1}$$

$$u = \int_0^z \rho w dz \tag{2}$$

$$W = W_o \left(\frac{P}{P_o}\right)^{\lambda} \tag{3}$$

$$T = T_o \left(\frac{P}{P_o}\right)^{\frac{\gamma R_{gas}}{g}} \tag{4}$$

Substituting the hydrostatic equation and (3) into (2) yields, after integration,

$$u = \frac{W_o P_o}{g(\lambda+1)} \left[1 - \left(\frac{P}{P_o}\right)^{\lambda+1}\right] \tag{5}$$

Solving (5) for (p/p_o) and substituting into (4) gives an expression for temperature as a function of the water vapor profile.

$$T = T_o \left[1 - \frac{g(\lambda+1)}{W_o P_o} u\right]^{\frac{\gamma R_{gas}}{g(\lambda+1)}} \tag{6}$$

Raising each side of (6) to the fourth power and multiplying by the Stefan-Boltzman constant gives the black-body radiance.

$$B(T) = B(T_o)\left[1 - \frac{g(\lambda+1)}{W_o P_o} u\right]^{\frac{4\delta R_{gas}}{g(\lambda+1)}} \tag{7}$$

The general transfer equation for a gaseous atmosphere is of form

$$R = -\int_o^{u_o} B(T) \frac{\partial \tau}{\partial u} du . \tag{8}$$

Let us assume $\tau = e^{-ku}$.

Then

$$\frac{\partial \tau}{\partial u} = -ke^{-ku} . \tag{9}$$

Substituting (7) and (9) into (8) yields an expression for the irradiance at any level in the atmosphere.

$$R = \int_{u=0}^{u=u_o} B(T_o) ke^{-ku}\left[1 - \frac{g(\lambda+1)}{W_o P_o} u\right]^{\frac{4\delta R_{gas}}{g(\lambda+1)}} du \tag{10}$$

Equations analogous to (10) may be written for the upward and downward irradiance at the top and bottom of each layer under consideration.

If we assume atmospheric radiation to be grey, we may begin a computation for any level with an irradiance from a preceeding calculation. We rewrite (10) as

$$R = \int_{u=0}^{u=u_o} B(T_o) ke^{-ku}\left[1 - \frac{g(\lambda+1)}{W_o P_o} u\right]^{\frac{4\delta R_{gas}}{g(\lambda+1)}} du + e^{-ku} R_o . \tag{11}$$

where R_o is the upward irradiance at the bottom of the layer when R is the upward irradiance, or R_o is the downward irradiance at the top of the layer when R is the downward irradiance. For upward irradiance calculations, the optical mass represented by "u" in the bracketed term in (11) must be replaced by $(u_o - u)$. All integrations of (11) were carried out by Gaussian quadrature.

It is helpful to examine (11) to learn how the effects of the various optically active atmospheric constituents are taken into account. Water vapor, u, appears explicitly in (11). As u increases, the divergence of irradiance increases. The effects of the other atmospheric constituents are incorporated into the effective absorption coefficient, K. The effects of clouds require larger K values, thus smaller transmissivities.

Since the optical mass of carbon dioxide between any two pressure surfaces is assumed constant, we may think of carbon dioxide as having the effect of a systematic increase in the K value. A larger K value results in a smaller transmissivity, which one expects in the presence of an additional absorbing gas. The radiative effects of ozone in the large tropospheric layers of this model are less than 1% of the radiative consequences of water vapor and carbon dioxide. Even so, one can assume a mean profile for ozone and employ the same logic as was used for carbon dioxide.

Figure 2 shows a schematic diagram of the model used in this study. Although cooling was calculated only for the two lowest layers, the third layer was necessary to calculate the downward irradiance at 200 mb. Equation (11) was solved for a K value for each layer, first from the observations of the upward irradiance and then from the

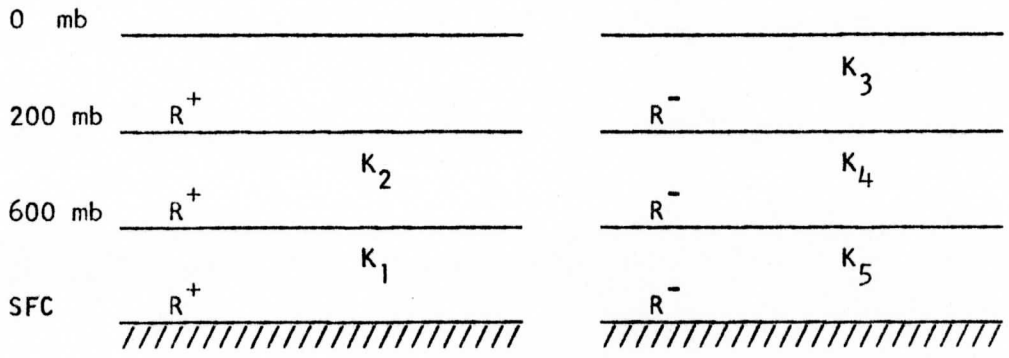

FIGURE 2. Schematic representation of infrared model.

downward irradiance. It was necessary to solve for two K's for each layer because of the differences in the spectral energy distributions of the upward and downward irradiances. We may attribute these differences to a different temperature history, a different distribution of absorbing gases and a vastly different background. The layer 0-200 mb was assigned only one K, resulting from the downward irradiance stream. Since cooling was not computed for this layer, it was not necessary to solve for a K from the upward stream.

Equation (11) was evaluated for the five effective absorption coefficients, and the resulting K's for 300 radiation sonde ascents were subjected to a multiple linear regression analysis using temperature and moisture parameters as independent variables.

An attempt to fit the entire set of data with one set of regression equations yielded unsatisfactory results. Therefore, the data was divided into three groups according to the slope of the sounding on a Rossby diagram. A simple finite difference calculation, $\Delta\theta_d/\Delta w$, for the surface to 200 mb layer was sufficient for classification. The multiple linear regression analysis was then repeated for each of the data groups given in Table 2. Figure 3 illustrates the grouping of the data on a Rossby diagram.

The independent variables in the regression equations were selected using a method described by Johnson (1965) based on the relative change of the residual sums of squares and its variance as a function of the number of independent variables. The resulting regression equations are of the form

$$K = A_o + A_1X_1 + A_2X_2 + \ldots + A_nX_n . \qquad (12)$$

DATA SET	LIMITS OF $\Delta\theta_d/\Delta w$ (in $^{o}K\ Kg\ g^{-1}$)
1	< -10.0
2	-3.5 to -10.0
3	> -3.5

TABLE 2. Limits defining three data sets for regression analysis.

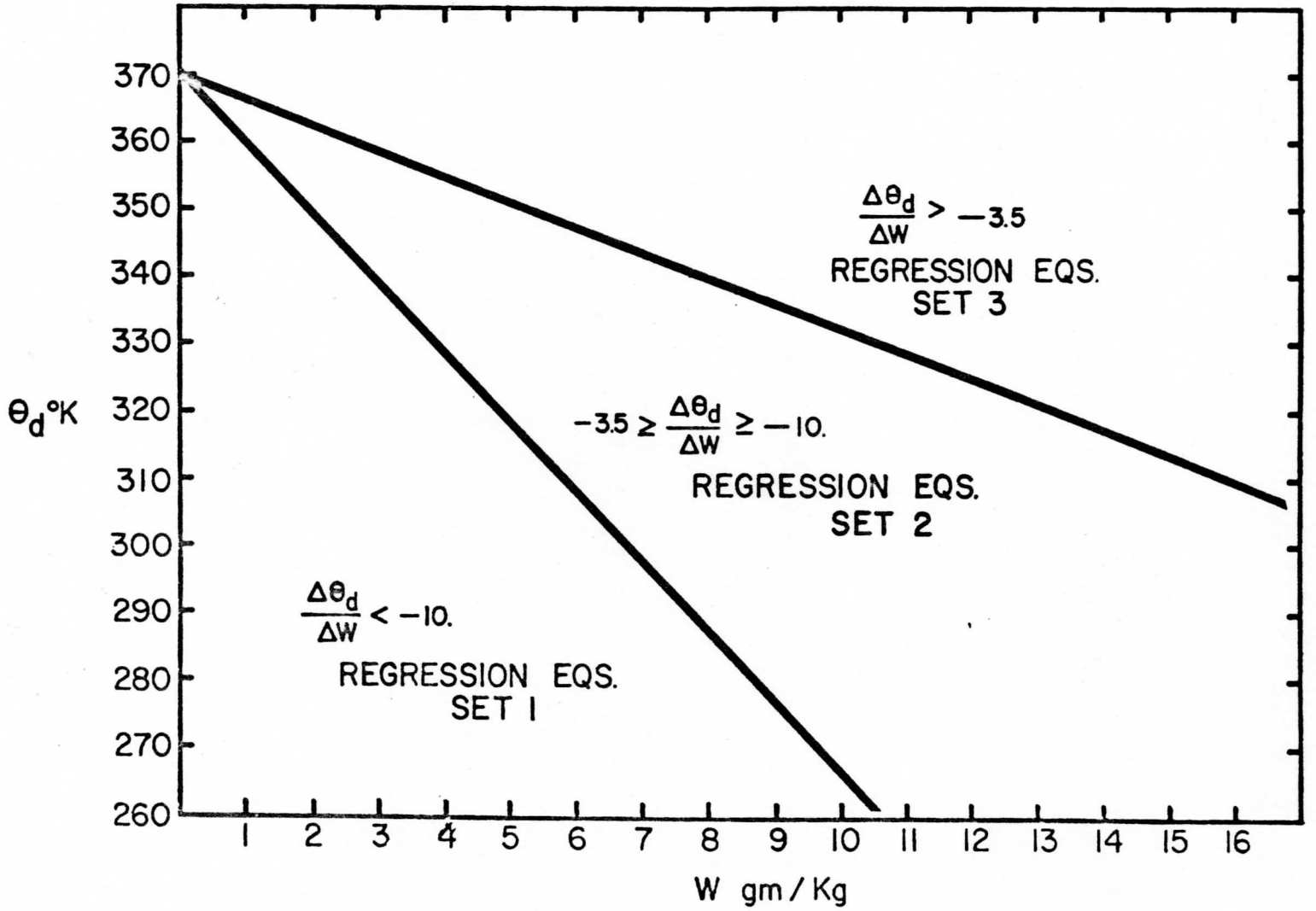

FIGURE 3: Rossby diagram illustrating divisions of data used in the infrared model.

The values of the coefficients, A_i, are given in Table 3 and the parameters, X_i, in Table 4 for each of the three data sets.

In order to use the results of this study, one applies the regression equations to find the K's and then uses (11) to determine the upward and downward irradiances at the surface, 600 mb and 200 mb levels. The upward irradiance at the surface was assumed to be the black-body irradiance evaluated at shelter temperature for a surface emissivity equal to 1.0. With the five irradiances calculated from (11), one can compute the mean infrared cooling of a layer from

$$\frac{\Delta T}{\Delta t} = -\frac{g}{C_p}\frac{\Delta R_N}{\Delta p} \quad . \tag{13}$$

Special consideration must be given to the case of a surface temperature inversion. In the presence of a strong surface temperature inversion, the infrared cooling of the surface to 600 mb layer would be greater than the radiation model will estimate. This would occur because the radiative input at the base of the layer would be considerably less than the shelter-temperature black-body irradiance. If the radiation model were made up of more, thus smaller, layers, the effect would be larger. To compensate for the inversion effect, we set the upward surface irradiance equal to the interface irradiance and solve for the lapse rate from an assumed surface temperature set equal to the mean temperature of the inversion layer. In this way the primary effect of a large surface temperature inversion, strong radiative cooling in the lower layer, is realized without significantly adding to the complexity of the model.

	A_0	A_1	A_2	A_3	A_4	A_5	A_6
Data Set 1	$\Delta\theta_d/\Delta w < -10.0$						
K(SFC-600)	8.8083	-.3157	-.7291	5.0351	1.2398	1426.6715	
K(600-200)	9.8867	.2514	-5.3278	-1.4084	2217.5211	.0286	
K(0-200)	-125.8305	.1550	-.2986	17.1303	-1.5071	9525.1979	.0079
K(200-600)	10.1866	-.1186	2.8233	-23.0199	-.0517		
K(600-SFC)	4.2265	.0268	2.8328	-3.7080	181.0553	-11.9336	
Data Set 2	$-3.5 \geq \Delta\theta_d/\Delta w \geq -10.0$						
K(SFC-600)	1.3859	-.0307	-108.4951	.3490	-.0041		
K(600-200)	26.7253	-7.6780	-3.4249	-.0241			
K(0-200)	-.7485	-1.2619	-91.5774	451.7000	214051.8380		
K(200-600)	-28.6231	1.1686	436.6048	-1.0294	16.8626		
K(600-SFC)	.4837	-.2050	244.0343	-.0021			
Data Set 3	$\Delta\theta_d/\Delta w > -3.5$						
K(SFC-600)	3.1456	.1686	-219.9099	.1709	.0872	-.0992	
K(600-200)	4.8202	-385.2431	.3474	.0438			
K(0-200)	-703.3311	34.4577	-41.5148	64.3894	-675903.6560		
K(200-600)	-478.6317	.4537	1774.2838	13.8258	.9688	.0044	-.0454
K(600-SFC)	-15.5254	.0539	.6112	.2743	-.4395	-745.2183	

TABLE 3. Infrared model regression coefficients.

	X_1	X_2	X_3	X_4	X_5	X_6
Data Set 1 $\Delta\theta_d/\Delta w < -10.0$						
K(SFC-600)	T(SFC)	W(800)	U(SFC-600)	λ(SFC -600)	γ(600-200)	
K(600-200)	W(SFC)	W(400)	γ(SFC-200)	γ(0-200)	$\lambda(600\text{-}200)^3$	
K(0-200)	PMSL	T(800)	U(SFC-600)	T(200)	γ(600-200)	$\lambda(SFC\text{-}600)^3$
K(200-600)	T(800)	U(600-200)	γ(600-200)	λ(600-200)		
K(600-SFC)	T(SFC)	W(600)	U(SFC-600)	γ(SFC-600)	U(600-200)	
Data Set 2 $-3.5 \geq \Delta\theta_d/\Delta w \geq -10.0$						
K(SFC-600)	T(800)	γ(SFC-600)	λ(SFC-600)	$\lambda(SFC\text{-}600)^3$		
K(600-200)	W(400)	γ(SFC-200)	$\lambda(600\text{-}200)^3$			
K(0-200)	T(800)	U(SFC-600)	U(600-200)	γ(0-200)		
K(200-600)	U(SFC-600)	γ(SFC-600)	T(400)	U(600-200)		
K(600-SFC)	U(SFC-600)	γ(SFC-600)	$\lambda(SFC\text{-}600)^3$			
Data Set 3 $\Delta\theta_d/\Delta w > -3.5$						
K(SFC-600)	T(SFC)	γ(SFC-600)	λ(SFC-600)	T(200)	λ(600-200)	
K(600-200)	γ(SFC-200)	λ(SFC-200)	$\lambda(600\text{-}200)^3$			
K(0-200)	W(SFC)	T(800)	λ(600-200)	γ(200-0)		
K(200-600)	PMSL	γ(SFC-600)	U(600-200)	λ(600-200)	$\lambda(SFC\text{-}600)^3$	$\lambda(600\text{-}200)^3$
K(600-SFC)	T(SFC)	U(SFC-600)	λ(SFC-600)	T(200)	γ(SFC-200)	

TABLE 4. Infrared model regression parameters.

3.2 Results

Ideally an empirical model of infrared cooling would reproduce exactly the observed cooling of an independent set of data. However, it would be naive to expect such perfection since the model is not perfect and the independent data not entirely free from error. For application in a numerical general circulation model, one can tolerate error in individual estimates of cooling as long as certain conditions are met.

Applying the model to an independent data sample, we have compared the observed and calculated infrared cooling rates under consideration of the following five properties.

1. Planetary mean value
2. Zonal or latitudinal mean value
3. Variation about zonal mean
4. North-South gradient
5. Vertical distribution

Let us briefly examine why these particular properties were selected. The planetary infrared cooling in a general circulation model must equal the absorbed solar energy or the model will show unrealistic changes of planetary temperature. A comparison of observed and calculated radiative cooling will indicate if any adjustment is necessary to maintain a realistic mean temperature.

Another test of the radiative cooling model is based on the concept of generation of available potential energy. Generation may be divided into two parts, a zonal component associated with the mean latitudinal radiative cooling, and an eddy component, associated with deviations from the mean radiative cooling. This division provided a convenient

means of comparing the infrared cooling model results with observations. Assuming that similar infrared radiative cooling means and deviations from the mean will have corresponding effects on the generation, we divided the radiative cooling rates into two parts, a latitudinal mean and a deviation from the mean. In this way the latitudinal means and their root mean square deviations of radiative cooling provide a test of the cooling model's potential effects on the generation of available potential energy in a general circulation model.

While the zonal means and their deviations represent the latitudinal properties of the infrared cooling rate, we also examined the north-south gradient of infrared cooling because of its role in determining the meridional exchange of heat required to maintain realistic north-south temperature gradients. This north-south exchange of heat energy is a basic feature of the atmosphere's circulation and must be preserved in a numerical model.

The final characteristic of the infrared cooling model that we examined is the vertical distribution of cooling. Since numerical models of the atmosphere are sensitive to the static stability, it is necessary to examine the stability change produced by infrared cooling.

Two sets of independent radiation sonde data were available for testing the infrared method. One set included ascents having maximum geographical and time coverage and the other set represented an intensive series of radiation sonde ascents during the passage of a mature extratropical cyclone through the central United States.

3.21 Extended Geographical Distribution Check

The nearly five hundred radiation sonde ascents used in this check represent five different geographical regions and all four seasons. All data at $3^{o}S$ were collected from Canton Island, and the $13^{o}N$ data were from Guam. The data for latitudes 32^{o}, 38^{o} and $44^{o}N$ were collected in southern, central and northern United States, respectively.

Tables 5a and 5b show a comparison of the observed and calculated radiative cooling using the five characteristics mentioned above. The zonal means are tabulated at five different latitudes which were chosen because of the unequal distribution of the observations. While there is satisfactory agreement at higher latitudes, the calculated cooling for both layers is less than the observed at lower latitudes. The calculated infrared result corresponding to the planetary mean differs from the observed by $0.13^{o}C\ day^{-1}$ in the surface to 600 mb layer and by $0.01^{o}C\ day^{-1}$ in the 600 to 200 mb layer.

The $0.13^{o}C\ day^{-1}$ discrepancy noted in the lower layer is due to the calculations at lower latitudes. The disagreement noted in the tropics would result in a relative warming of the atmosphere and is especially important since the tropics represent a significant fraction of the earth's surface area. A comparable error at high latitudes would have a much smaller effect on a general circulation model because the area involved would be much smaller. In order to keep a general circulation model from "overheating" in the tropics, one could add a bias to the computed cooling. The magnitude of such a bias would be determined in one of two ways. By observing a numerical model's response to the present infrared model, one could experiment and arrive at a bias that would result in a realistic temperature field. A second method

Surface - 600 mb Layer

Latitude	No. of Soundings	Calculated			Observed		
		Mean Cooling °C/Day	RMS Deviation °C/Day	N - S Gradient °C/Day/°Lat	Mean Cooling °C/Day	RMS Deviation °C/Day	N - S Gradient °C/Day/°Lat
44°N	80	1.34	.47		1.35	.89	
				.04			.04
38°N	230	1.60	1.35		1.59	.91	
				-.07			-.12
32°N	50	1.19	1.10		.89	1.20	
				.04			.09
13°N	60	1.87	1.50		2.53	1.20	
				-.00			-.02
3°S	60	1.82	.82		2.18	.69	
Mean		1.61	1.18	.01	1.74	.99	.02

TABLE 5a. Comparison of observed and calculated infrared radiative cooling characteristics for extended geographical distribution check.

500 - 200 mb Layer

Latitude	No. of Soundings	Calculated			Observed		
		Mean Cooling °C/Day	RMS Deviation °C/Day	N - S Gradient °C/Day/°Lat	Mean Cooling °C/Day	RMS Deviation °C/Day	N - S Gradient °C/Day/°Lat
44°N	80	1.40	.87		1.15	.56	
				-.04			.00
38°N	230	1.17	1.02		1.17	.69	
				.14			.08
32°N	50	2.03	1.21		1.65	1.10	
				-.03			-.01
13°N	60	1.40	1.35		1.56	1.15	
				.01			.02
3°S	60	1.56	1.41		1.89	.64	
Mean		1.30	1.09	.00	1.31	.77	.01

TABLE 5b. Comparison of observed and calculated infrared radiative cooling characteristics for extended geographical distribution check.

would be to make additional tropical radiation measurements and determine the mean infrared cooling rates for the tropical latitudes. Then a simple subtraction of the radiation technique's results from the observed mean would give the bias. Additional measurements would also allow further development of the infrared model and may make an adjustment unnecessary.

There are two likely reasons for the technique working better at midlatitudes than in the tropics. In the midlatitudes high and low pressure systems have characteristic moisture, temperature and cloud features. A high pressure system characteristically has dry, cloud-free air, and a low pressure system has moist, cloudy air. There appears to be an adequate relationship in the midlatitudes between moisture, temperature and cloudiness to infer the radiative effects of clouds. In the tropics we find remarkably little variation in the moisture and temperature fields; however, ESSA and ATS satellite photographs have shown large variations in tropical cloud structure and cloud coverage. Since the moisture and temperature characteristics of clear and cloudy conditions in the tropics are very similar, a given set of temperature and moisture parameters apparently does not define unique radiative properties. This lack of relative uniqueness could account for the radiation model working better at higher latitudes than in the tropics.

Since the temperature and moisture profiles do not appear to be adequately sensitive to the sky condition, we should attempt to find another parameter that will be sensitive. Perhaps the "y" intercept of the Rossby diagram profile is related to the cloud structure and, or, distribution. This possibility will be explored in future research.

Another important difference between the midlatitude and tropical cases is the amount of available data. Nearly four times as many

radiation ascents were available from the middle latitudes as from the tropics. This disparity in geographical representation of the data is accentuated if we consider the areas represented by a zonal ring in the tropics and a zonal ring in the middle latitudes. The tropical ring is much larger; thus we are using fewer measurements to represent a significantly larger area. Figure 4, an ATS photograph of the Pacific Ocean, dramatically illustrates the variance in cloud conditions at tropical latitudes. We have indicated the positions of Guam and Canton Island on the photograph. It is quite obvious that the data taken at these two stations cannot necessarily be assumed representative of all tropical latitudes.

The root mean square deviations between observed and calculated infrared cooling rates were 34% and 26% of the mean observed cooling rates in the tropics and middle latitudes, respectively. If the deviations were normally distributed, a 30% root mean square deviation would have little effect on a numerical general circulation model. The numerical model will not react quickly to one, or several, erroneous radiative cooling estimates because the model acts as a smoothing filter. It will react to the mean cooling. Since the numerical model calculates many cooling rates as a function of time and space, the standard error of the mean cooling rate will be very small. The good agreement of the observed and computed mean cooling at 38° latitude in Tables 5a and 5b illustrates the effect of a large data sample.

The meridional gradient was computed by differencing the zonal means and dividing by the latitude increment. The signs of the gradients agree for all comparisons except for the 600 to 200mb layer between 44°N and 38°N. This difference is caused by the overestimate of the calculated cooling at 44°N.

FIGURE 4: ATS photograph illustrating variation of cloud coverage, cloud heights and cloud type in the tropics.

The relative agreement of the vertical distribution of cooling is satisfactory except at 44^{o}N where the lower layer, relative to the upper layer, is observed to cool 0.20^{o}C day^{-1} while it is computed to warm 0.06^{o}C day^{-1}.

3.22 Synoptic Check

A primary objective of this study was to provide a method capable of representing synoptic scale radiation fields in a numerical model. Fifty-six radiation sonde ascents were made on December 12, 1965, during the passage of an extratropical cyclone. These ascents were made at fourteen midwestern United States Weather Bureau upper air stations. Figure 5 shows the synoptic situation on December, 12, 1965, at 00 and 1200 GMT. The radiation cooling data were gridded, and smoothed in the process, on a 2^{o} latitude by 2^{o} longitude grid for both the observed and calculated cases.

Tables 6a and 6b show a comparison of calculated and observed cooling rates employing the five characteristics. The mean observed cooling over all latitudes for both layers exceeded by 10-20% the calculated rate. The root mean square deviation for the calculated cooling was less than for the observed, indicating some smoothing effect.

Mean zonal calculated cooling for both layers agreed well with the observed. The root mean square deviations about the zonal means indicated a smoothing as did the deviation about the total mean. The calculated mean north-south gradient, 0.15^{o}C day^{-1} $(2^{o}$ lat$)^{-1}$, agreed well with the mean observed gradient for the lower layer, 0.10^{o}C day^{-1} $(2^{o}$ lat$)^{-1}$. For the upper layer, the observed mean gradient was -0.11^{o}C day^{-1} $(2^{o}$ lat$)^{-1}$, and the calculated was -0.13^{o}C day^{-1} $(2^{o}$ lat$)^{-1}$.

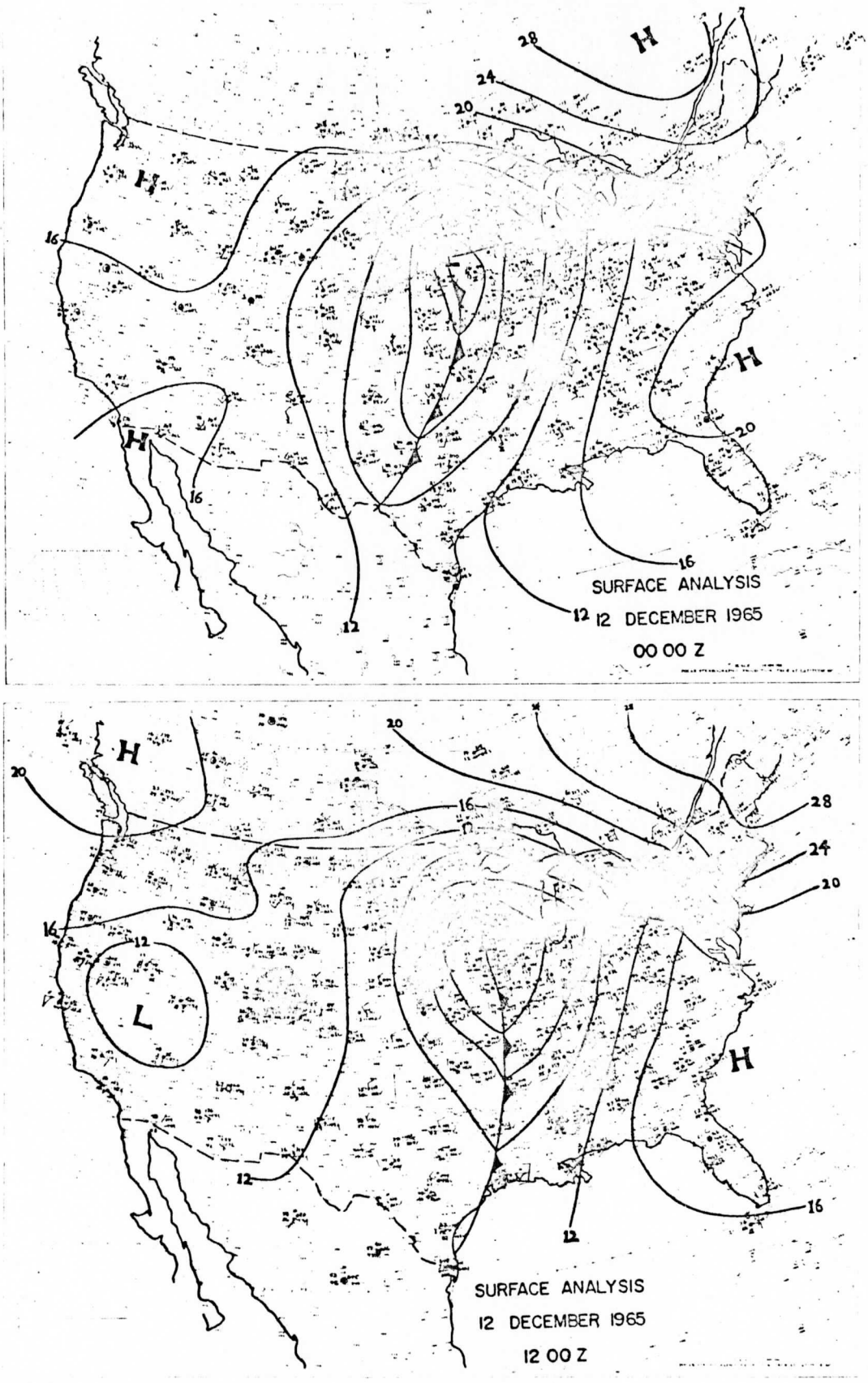

FIGURE 5: Surface pressure map of United States, December 12, 1965, 00 and 1200 GMT.

Surface to 600 mb Layer

Latitude	Calculated			Observed		
	Mean Cooling °C/Day	RMS Deviation °C/Day	N - S Gradient °C/Day/2°Lat	Mean Cooling °C/Day	RMS Deviation °C/Day	N - S Gradient °C/Day/2°Lat
48°N	.90	.15		.48	.55	
47			.24			.47
46	1.14	.19		.95	.48	
45			.34			.61
44	1.48	.34		1.56	.68	
43			.00			-.07
42	1.48	.19		1.49	.33	
41			.03			-.21
40	1.51	.19		1.29	.46	
39			-.18			-.20
38	1.33	.24		1.08	.56	
37			.03			.08
36	1.36	.37		1.16	.39	
35			.26			.07
34	1.62	.41		1.23	.30	
33			.48			.05
32	2.10	.77		1.28	.49	
Mean	1.45	.48	.15	1.23	.84	.10

TABLE 6a. Comparison of observed and calculated infrared radiative cooling characteristics for synoptic check.

600 - 200 mb Layer

Latitude	Calculated			Observed		
	Mean Cooling °C/Day	RMS Deviation °C/Day	N - S Gradient °C/Day/2° Lat	Mean Cooling °C/Day	RMS Deviation °C/Day	N - S Gradient °C/Day/2° Lat
48°N	2.22	.27		1.98	.27	
47			-.34			-.46
46	1.88	.31		1.52	.48	
45			-.36			-.26
44	1.52	.47		1.26	.18	
43			.09			.27
42	1.61	.41		1.53	.26	
41			.01			.10
40	1.62	.45		1.63	.19	
39			.23			-.14
38	1.85	.35		1.49	.23	
37			-.14			-.13
36	1.71	.26		1.36	.30	
35			-.13			-.08
34	1.58	.16		1.28	.31	
33			-.39			-.16
32	1.19	.27		1.12	.21	
Mean	1.74	.71	-.13	1.46	.39	-.11

TABLE 6b. Comparison of observed and calculated infrared radiative cooling characteristics for synoptic check.

A tendency to create instability due to the cooling of the upper layer relative to the lower layer was present in both the observed and calculated rates. The results tabulated in Tables 6a and 6b indicate that the model can produce realistic synoptic detail of infrared cooling patterns. While absolute agreement was not attained, both the signs and magnitudes of the characteristics show good agreement.

4. Shortwave Model

In order to have a complete method to simulate radiation cooling and warming in a cloudy atmosphere, we have utilized a technique given by Hanson, et al. (1967) for the absorption of solar radiation in the atmosphere. Hanson used data from a United States network of pyranometers, radiosonde ascents and the Tiros IV satellite to arrive at (14) for the fractional solar absorption of the atmosphere. Let $u^* = u \sec \theta(t)$.

$$q_a = .096 + .045 \left[u^*\right]^{1/2} \ln_e u^* \qquad (14)$$

Hanson's equation refers to the whole column of atmosphere between the satellite and the ground. In arriving at (14), Hanson assumed zero water vapor above the $-40^{\circ}C$ level.

In agreement with estimates by Fritz (1950), 0.03 was subtracted from (14) to account for absorption by ozone and water vapor above 200 mb. We assumed the fractional absorption was distributed with height according to the relationship expressed by

$$q_a' = q_a - .03 = 1 - e^{-Du^*}. \qquad (15)$$

When applying (15), u^* was made zero at 200 mb and equal at the surface to the total optical path for the surface to 200 mb layer. Solving (14) for q_a and then (15) for the constant, D, gives an expression for the vertical distribution of shortwave absorption.

Equation (16) was then used to calculate the energy absorbed in the two layers, 200 to 600 mb and 600 mb to the surface.

$$E = S\int_{t_1}^{t_2} \cos\theta\{t\}\left(1 - e^{-Du\sec\theta\{t\}}\right)dt \qquad (16)$$

S represents the solar constant and $\theta(t)$ the zenith angle of the sun at time, t. The solar warming can then be computed from

$$\frac{\Delta T}{\Delta t} = \frac{g}{C_p}\frac{E}{\Delta p} \; . \qquad (17)$$

Vonder Haar, et al. (1967) describe results obtained by applying (13) to London's (1957) climatological water vapor data. They compared London's estimates of solar absorption with those from (13) and found that London's value for the mean annual Northern Hemisphere solar absorption was 32% smaller. London and Vonder Haar show good agreement at midlatitudes; however, London's values are 42% smaller and 37% greater in the tropics and at high latitudes, respectively. In view of the difference between London's and Vonder Haar's results, it would be advisable to repeat Hanson's computation for different geographical regions as data becomes available.

Vonder Haar applied (15) to partition the absorbed solar energy in the vertical and compared his results with Davis (1963). His results showed larger amounts of energy absorbed in the surface to 600 mb layer than Davis reported. Such increased heating from below, coupled with the larger total absorption reported by Hanson, would result in a tendency for increased convective activity. A numerical general circulation model would be sensitive to such an arrangement of heating.

Figure 6 represents the results of applying (16) to moisture

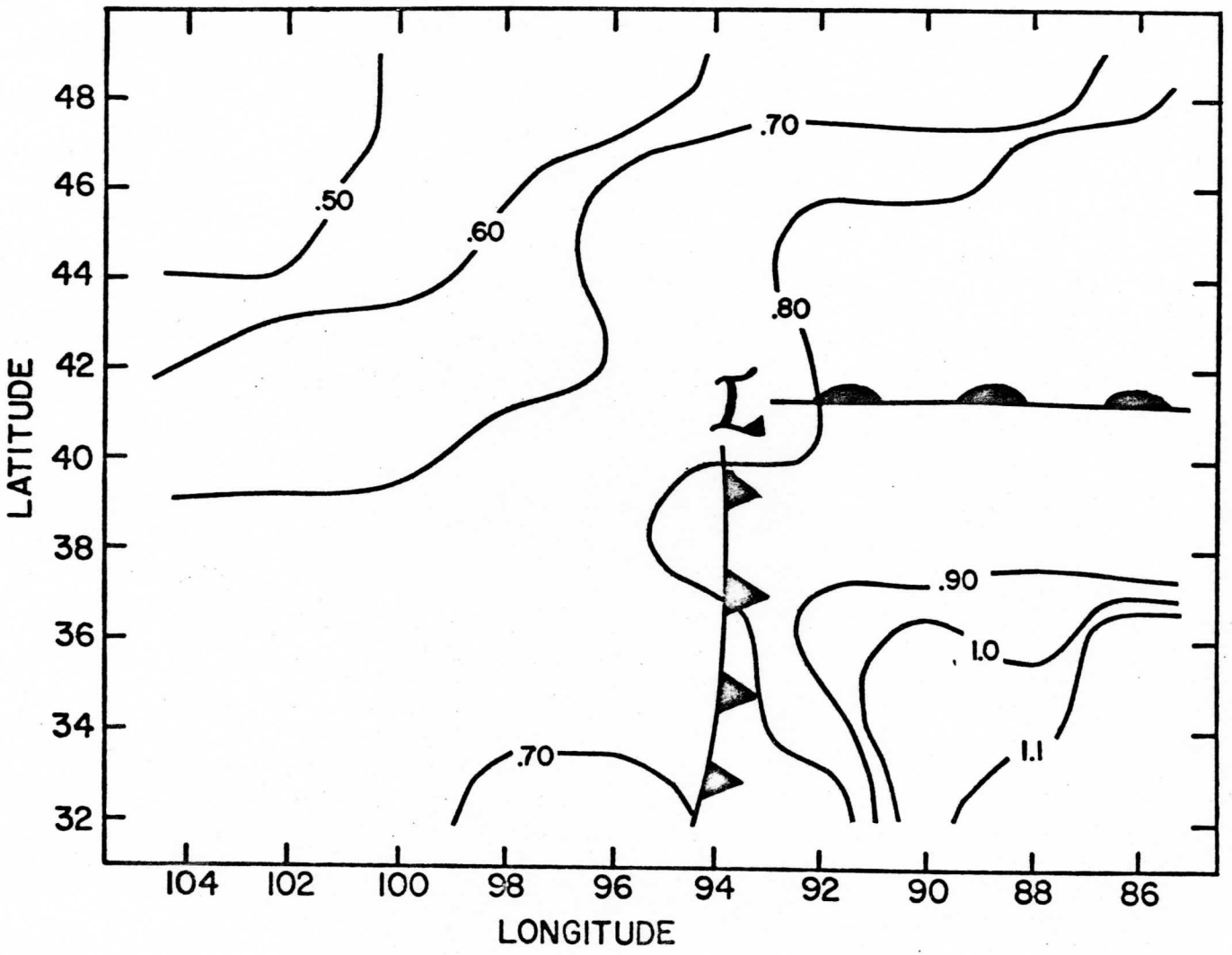

FIGURE 6: Synoptic scale distribution of solar warming ($^{o}C\ day^{-1}$) of the surface to 600 mb layer for December 12, 1965.

data for the surface to 600 mb layer over the midwestern United States on Decenber 12, 1965. The synoptic situation was dominated by a mature extratropical cyclone centered at 41°N latitude and 94°W longitude, with warm and cold fronts extending due east and south, respectively. The spatial representation of shortwave warming appears as one would expect, reflecting the moisture distribution classically associated with an extratropical cyclone.

5. Application of the Models

Figure 7 is a flow diagram outlining the steps in the application of the infrared and shortwave models. The two techniques, infrared and solar, may be applied either separately or together.

While this study is based on a two-level model for infrared and shortwave radiation, both methods may be extended for use in a three, or more, level model. As more levels are added, computation time correspondingly increases. The user must decide how much vertical detail is required for a given application.

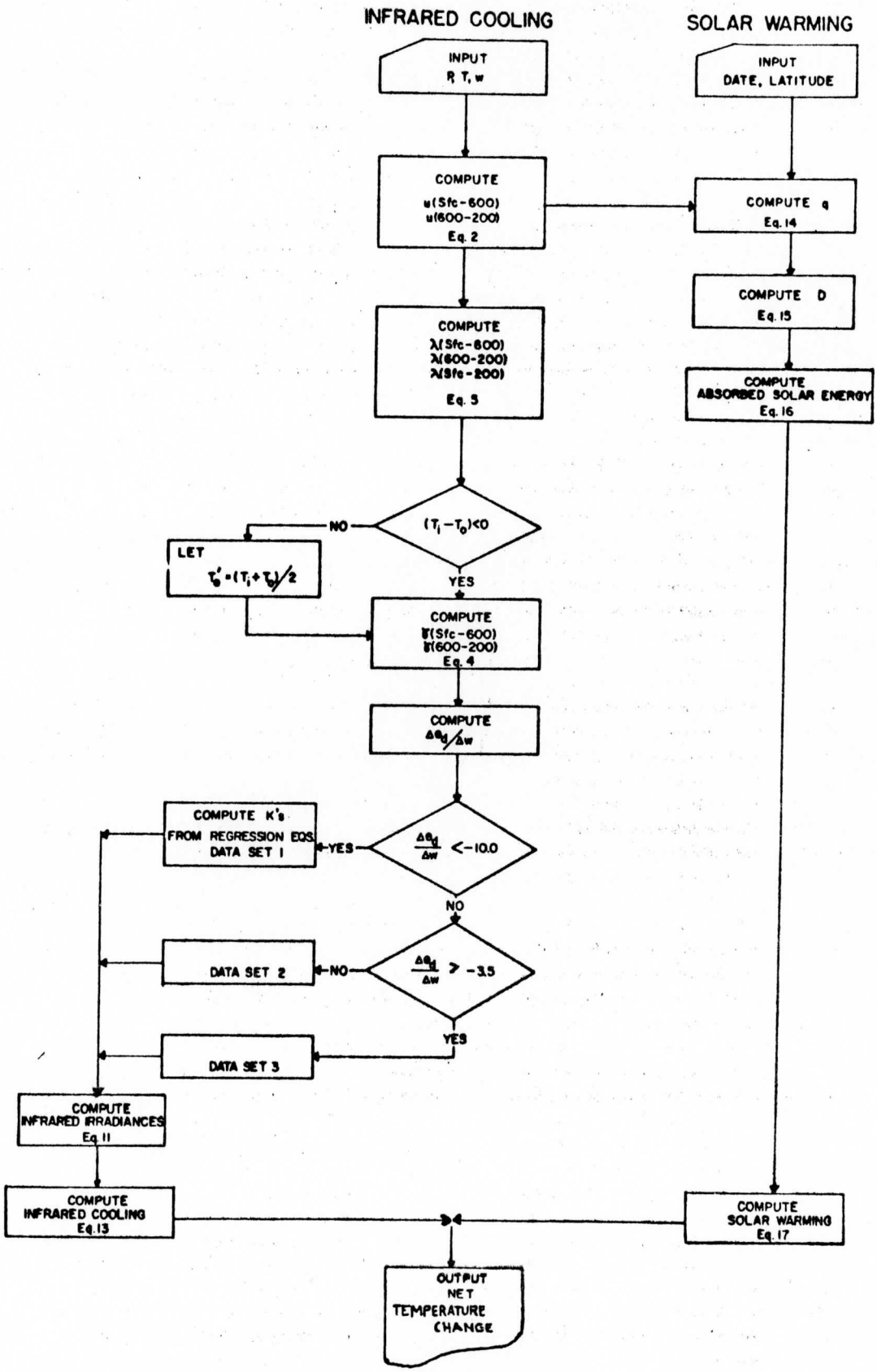

FIGURE 7: Flow chart for infrared and solar radiation models.

6. Conclusions

This study describes a means to include the effects of clouds on solar and longwave radiation transfer in a primitive equation numerical general circulation model where moisture is carried as a dependent variable. Specific information on cloudiness is not required even though the radiation results include the likely effects of clouds. The infrared technique can produce synoptic-scale radiative cooling patterns. The root mean square deviation between observed and calculated daily cooling rates is 34% for tropical data and 26% for midlatitudes. Because the errors in estimates for midlatitude situations in the test sample used are normally distributed, the error for the whole globe or for several days is likely to be very much less. An individual error of 30% in the application to a numerical general circulation model is not serious because the model acts as a smoothing filter. The data sample in the tropics was much more limited, and the errors departed from a normal distribution in a manner which will introduce a slight bias.

The technique to calculate solar warming is based on the method of Hanson, et al. (1967). The method takes the effects of clouds into account without relying on specific cloud information. The solar method has not been tested. Initial calculations suggest the technique may yield anomalously high solar absorption in tropical latitudes.

It should be noted that regression coefficients in this study were computed from a limited geographical data sample. Since several atypical latitude and climatic regions were represented, it may be unrealistic to assume the coefficients apply to the entire earth. The geographical representativeness of the coefficients and

parameters must be checked when additional data becomes available.

One further precaution on the use of the radiation models should be mentioned. The models can be expected to reproduce only average values of warming and cooling because they rely on a statistical relationship between temperature and moisture profiles and clouds. There will be instances when temperature and moisture profiles indicate a high probability of clouds but clouds will not be present. In such a case the models cannot give a realistic estimate of radiative warming rates. Non-water substance clouds, such as dust and volcanic debris, also affect radiative warming; however, these effects are not treated by the models presented in this study.

7. Future Research

The radiation model developed in this study is the first attempt to simulate the effects of clouds using water vapor and temperature profiles. The empirical relationship was obtained by treating actual radiation sonde observations in a manner which did not separate the effects of gaseous moisture from cloud particles. We found this simple relationship to be quite effective but additional study might improve the results. A better representation of radiation in the tropics is needed. The temperature and moisture profiles of tropical atmospheres show remarkably little change from day to day, and, therefore, the profile is not a sensitive indicator of the presence or absence of clouds. The depth of the moist layer might be more sensitive to cloud structure than the power law representation. A further subdividing of the data on the Rossby diagram might be useful. In the present study only the slope of the Rossby profile was used to divide the data; the "y" intercept may be sensitive to cloud conditions.

Cirrus clouds in the high tropical troposphere have a profound effect on the radiation budget. Some means must be found to account for them. Possibly the temperature of the upper troposphere since, according to Darkow (1963), low temperatures are conducive to long cirrus cloud lifetime.

Perhaps a better check on the radiation model's performance could be made by applying the model to radiosonde measurements and and comparing the computed upward irradiance at the top of the atmosphere with satellite observations. This would allow a far more general

evaluation of the model's performance since many more coincident satellite infrared measurements and radiosonde ascents are available than radiation sonde measurements.

References

Brooks, D. L., 1950: A tabular method for computations of temperature change by radiation in the free atmosphere. Journal of Meteorology, 7, p. 313.

Darkow, Grant, 1963: A study of infrared radiation measurements in the vicinity of cirrus clouds, Ph.D. Thesis, Department of Meteorology, University of Wisconsin.

Davis, Paul A., 1963: An analysis of the atmospheric heat budget, Journal of the Atmospheric Sciences, Vol. 20, No. 1 pp. 5-22.

Dutton, John A. and Donald R. Johnson, 1967: The theory of available potential energy and a variational approach to atmospheric energetics, Advances in Geophysics, 12, pp. 333-436.

Fritz, Sigmund, 1951: Solar radiant energy and its modification by the earth and its atmosphere, Compendium of Meteorology, American Meteorological Society, p. 20.

Hanson, Kirby J., Thomas H. Vonder Haar and Verner E. Suomi, 1967: Reflection of sunlight to space and absorption by earth and atmosphere over the United States during spring 1962, Monthly Weather Review, Vol. 95, No. 6, pp. 354-361.

Johnson, Donald R., 1965: The role of terrestrial radiation in the generation of available potential energy, Ph.D. Thesis, Department of Meteorology, University of Wisconsin.

Kuhn, P. M., 1964: Personal communication.

London, Julius, 1957: A study of the atmospheric heat balance. Final Report, Contract No. Af19(122)-165, Department of Meteorology and Oceanography, New York University, 99 pp.

Manabe, Syukuro, Joseph Smagorinsky and Robert F. Strickler, 1965: Simulated climatology of a general circulation model with a hydrologic cycle, Monthly Weather Review, Vol. 93, No. 12, pp. 769-798.

Mastenbrook, H. J., 1966: Water vapor observations at low, middle and high latitudes during 1964 and 1965, Naval Research Laboratory Report 6447, 201 pp.

Murgatroyd, R. J., 1957: Wind and temperatures between 20 km and 100 km - a review, Quarterly Journal of the Royal Meteorological Society, 83, pp. 417 - 421.

Suomi, Verner E. and William C. Shen, 1963: Horizontal variation of infrared cooling and the generation of eddy available potential energy, Journal of the Atmospheric Sciences, Vol. 20, No. 1, pp. 62 - 65.

Vonder Haar, Thomas H., Kirby J. Hanson and Verner E. Suomi, 1967: Absorption of solar radiation in the real atmosphere as a function of water vapor content, To be published.

Inadequacy of Conventional Radiosonde Baseline Procedures in the Tropics

STEPHEN K. COX, JAMES A. MAYNARD AND VERNER E. SUOMI

University of Wisconsin
Madison, Wisconsin

ABSTRACT

An analysis of tropical radiosonde temperature measurements made during the Line Island Experiment suggests that conventional radiosonde preflight procedures are inadequate in a remote tropical environment. Temperatures computed from conventional and modified baseline techniques are compared at five pressure surfaces, 1000, 800, 600, 400 and 200 mb. Temperatures obtained from the two baseline techniques showed an average deviation at 1000 mb of 0.96C for sixty-two soundings. These comparisons indicate that a careful examination of radiosonde calibration techniques is needed before large investments are made in future global experiments.

1. Introduction

In preparation for the Line Island Experiment, a data gathering effort in the tropics sponsored by NCAR in the Spring of 1967, we investigated ways of improving the accuracy of the upper air temperature measurements without making major modifications to conventional upper air equipment. A careful examination of the entire upper air system indicated that a most critical phase of an upper air sounding is the baseline check. The baseline check is a one point calibration, matching a blocking oscillator modulator to a thermistor and hygristor. While Hodge and Harmantas (1965) have mentioned several potential sources of temperature error in baseline procedures, we will discuss one point in detail which is particularily important in the tropics. The conventional radiosonde modulator suffers a decrease in resolution at both very high and very low temperatures. If one makes the baseline at either temperature extreme in the region of relatively low temperature-frequency response, he sacrifices the accuracy of the entire sounding. This is because each point in a temperature profile is evaluated using the baseline check point as a reference.

We propose that an expanded-scale baseline modulator be used to establish the temperature baseline for a radiosonde when the baseline must be conducted at high temperatures. The expanded scale precision baseline modulator is inexpensive and its use requires little additional effort on the part of the technician. There are other ways to accomplish a more accurate baseline check but they would require more modification to conventional upper air equipment.

2. Statement of the Problem

In routine radiosonde ascents a procedure called the baseline calibration is followed prior to flight in order to provide an absolute calibration of a

particular temperature-sensing thermistor used in conjuction with the particular blocking oscillator modulator unit in the radiosonde. This calibration procedure, spelled out in detail in the operations manuals (USWB (1957)) and followed meticulously by typical observers, is called the baseline check. Using high temperatures for baselining a radiosonde forces one to make the baseline in a relatively insensitive part of the temperature-frequency scale. The upper curve on Fig. 1 illustrates a typical frequency-temperature response of a conventional Weather Bureau modulator and air temperature thermistor. Since the slope of the curve is less at high temperatures, it is more difficult to resolve temperature accurately as a function of frequency.

Normally the baseline check is made at or above room temperature since conventional baseline check boxes do not include cooling devices. This places a severe constraint on tropical upper air data because high temperatures force one to perform the baseline on a relatively flat part of the upper curve in Fig. 1. As an example, let us take the extreme temperature range 40-50C which exhibits a mean slope of 0.3 ordinate/C. A careful observer can consistently read frequency to within 0.2 ordinate which, for this extreme temperature range, corresponds to 0.67C. For the 30-40C range, the uncertainty is 0.55C.

Our primary goal was to minimize the uncertainty in the temperature baseline check. A self-imposed constraint was that we utilize the standard upper air system and equipment with a minimum of modification.

3. Proposed Solution of the Problem

In order to assure high baseline calibration accuracy, a carefully calibrated, high sensitivity temperature-baseline modulator was used to baseline many of the Line Island Experiment radiosonde ascents. In essence this was

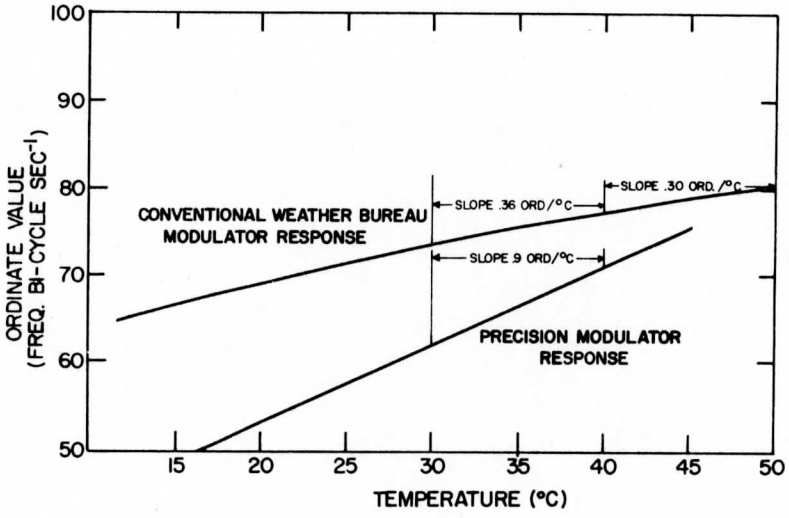

Fig. 1. Comparison of conventional and precision Weather Bureau modulator temperature-ordinate response.

simply a means to use a calibrated thermistor as a sensitive thermometer and a means to insert the thermistor to be used in the actual flight into a sensitive measuring circuit. All measurements were recorded on the strip chart as well. This baseline modulator was not used to make the sounding but only to baseline the conventional sonde.

Figure 2 is a partial schematic diagram of a baseline modulator designed to increase the slope of the frequency-temperature curve for the temperature range 10-50C. It is basically a conventional Weather Bureau radiosonde modulator and Military modulator with the resistors R_o, R_o' and capacitors C_1, C_1' changed to give a steeper frequency-resistance curve. The two baseline modulators are to be used with their respective type of radiosonde. We have also added the precision scaling resistors R_1, R_2, R_3 which servedto calibrate the resistance-frequency scale from which the baseline data were taken. While the modified circuit does draw approximately 0.4 milliamperes as compared to 0.2 milliamperes in the conventional sonde, tests revealed no detectable self-heating of the thermistor.

The lower line on Fig. 1 shows the temperature-ordinate relationship for the precision baseline modulator. The increase in sensitivity over the conventional sonde is obvious from a comparison of the slopes of the ordinate-temperature curves. For the temperature interval 30-40C the precision modulator gives a 2.5 times larger ordinate change for a given temperature increment than the conventional modulator, and 3.0 times greater ordinate change for the 40-50C interval. For the Military sonde, Fig. 3, the precision modulator yields 2.6 times the ordinate change that the conventional sonde gives for the 30-40C interval.

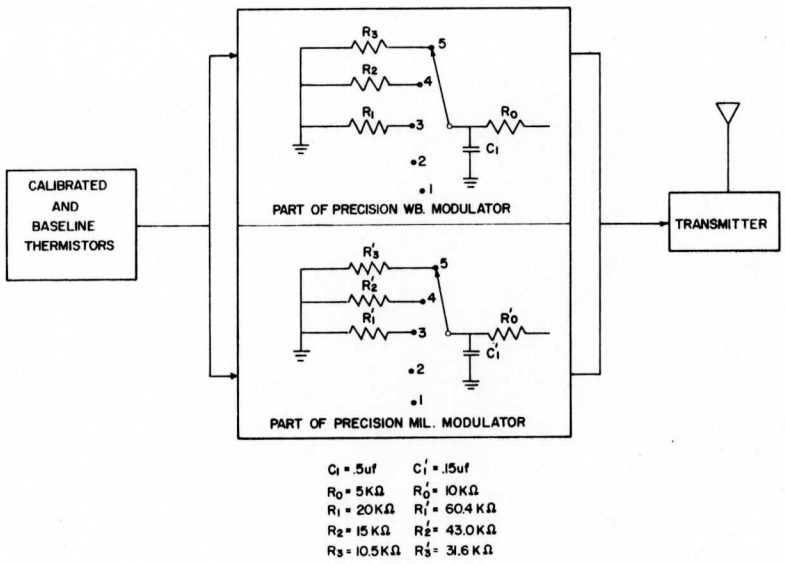

Fig. 2. Schematic diagram of the precision baseline modulator.

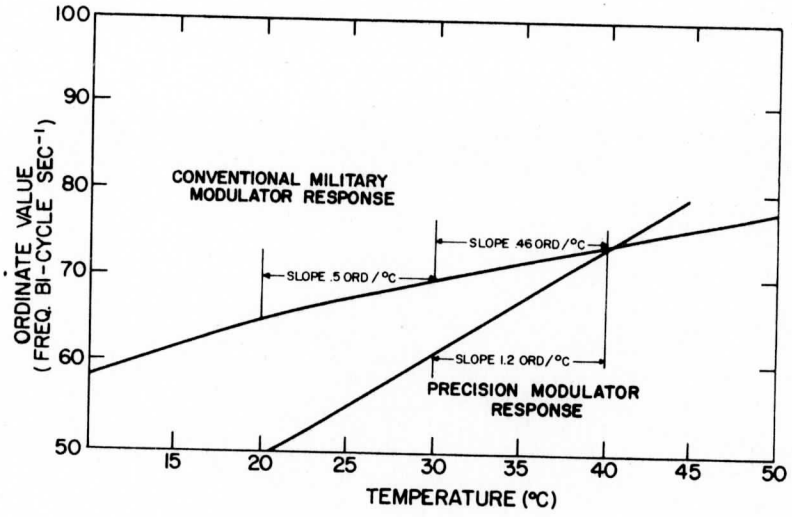

Fig. 3. Comparison of conventional and precision Military modulator temperature-ordinate response.

The modified baseline procedure used during the Line Island Experiment on many of the upper air soundings consisted of measuring a fixed known resistance with both the baseline modulator and the radiosonde modulator, and measuring the resistance of the radiosonde thermistor and of a calibrated thermistor held in close proximity to the radiosonde thermistor, with the baseline modulator. A calibrated Weather Bureau-type thermistor was used with the Weather Bureau baseline modulator and a calibrated Military-type thermistor with the Military version. All data from this baseline check were recorded directly on the strip chart recorder used to record the radiosonde data, providing a permanent record of the baseline temperature from the calibrated thermistor trace. One may refer back to this trace and check the baseline temperature, ex post facto.

Clearly the accuracy of this baseline system is dependent upon the precision of the original calibration of the calibration thermistor. This calibration may be performed under carefully controlled laboratory conditions and may be made quite accurate. It is certainly superior to the calibration which one makes in the conventional baseline where a thermometer is visually read under the pressure of a launch schedule and has less control over the physical conditions.

The new baseline information must be converted into a form compatible with the radiosonde temperature-frequency slide rule. Over the temperature range 15-45C, the baseline modulator frequency and the rod thermistor-measured temperature are linearly related and the temperature may be computed directly. The expanded scale frequency corresponding to the radiosonde thermistor may be converted into resistance from a frequency-resistance calibration of the precision modulator.

One may next apply (1) to compute the corresponding ordinate value for the conventional modulator.

$$f = R_3 f_o/(R_{thrm} - f_o KR_{thrm} + R_3 f_o K) \qquad (1)$$

In Eq. 1, K is the reciprocal of the low reference frequency and R_{thrm} is the resistance of the baseline thermistor as deduced from the precision modulator. A frequency-resistance calibration for each conventional sonde was established by placing a precision resistor, R_3 in Fig. 2, in place of R_{thrm} in the grid circuit of the sonde and recording the corresponding frequency, f_o. Substituting for R_3, R_{thrm}, and f_o into (1), one may solve for f, the conventional frequency corresponding to the temperature, T. Then f and T make up the temperature baseline point. While the above conversion may appear formidable, it may be simplified by using a specially constructed slide rule.

In order to expedite the baseline procedure in the field, we constructed a slide rule for the Weather Bureau baseline modulator which directly converts the new baseline information into conventional baseline parameters. Figure 4 shows this slide rule. It is utilized by first setting one calibration point on scales A and B which correspond to temperature and baseline modulator ordinate, respectively. Scales A and B are set once for a particular combination of a calibrated thermistor and baseline modulator and left unchanged until either the thermistor or baseline modulator is replaced. Scale C, which moves relative to scale B, enables one to convert from the precision baseline ordinate to a conventional ordinate value. The arrow at 75. on scale B must be aligned with the ordinate observed from the conventional sonde when the precision resistor R_3 is placed in the blocking oscillator grid circuit. This must be done for each sonde

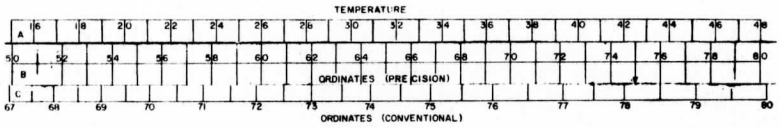

Fig. 4. Precision baseline slide rule for conversion of precision baseline data into conventional baseline parameters.

baselined.

The total procedure of making the precision baseline and converting to conventional baseline parameters adds approximately four minutes to the preflight preparation normally made for a radiosonde ascent.

4. Results

The Line Island Experiment offered an opportunity to test the new baseline technique in a tropical field experiment. The high temperatures and humidities provided the extreme environmental conditions to make conventional baselining techniques inadequate. Conventional baseline procedures call for a carbon hygristor element to be calibrated at values between 20 and 40 percent relative humidity, hardly typical of a tropical environment. In the Line Island Experiment chemical desicants were not adequate to reduce the relative humidity to the desired level so the calibration box was heated in order to lower the relative humidity to the prescribed value. While this procedure met the requirements for the relative humidity baseline, it had a serious detrimental effect on the temperature baseline, forcing the use of the flat part of the temperature-ordinate scale for the baseline calibration. The mean conventional baseline temperatures at the Palmyra and Christmas Island stations were 39.9C and 42.2C respectively.

Thirty-nine Christmas Island soundings and twenty-three Palmyra soundings were evaluated using both the modified and conventional baseline techniques. The only variable between the modified and conventional evaluations was the temperature baseline; both evaluations were made from the same ordinate input data.

The precision and the conventional baseline techniques have been compared in two ways. The temperatures obtained from the two different baseline techniques at various levels were subtracted and table 1 presents the average deviations for the Palmyra and Christmas Island soundings. The average deviation for the 1000 mb surface was 0.59C and 0.35C at 200 mb for the Palmyra soundings and 1.17C at 1000 mb and 0.75C at 200 mb for Christmas Island.

The average deviation and the arithmetic average deviation for the Christmas Island data are relatively close, however for Palmyra the two differ markedly. The small arithmetic average deviation for Palmyra indicates that the deviation tends to be random. The lower resolution of the conventional sonde would tend to induce a random error on the temperature data since the observed baseline ordinate is as likely to be too high as too low. That this is not the case of the Christmas Island data indicates the presence of a systematic error.

A possible explanation for the systematic error is that a temperature gradient existed between the thermistor and the thermometer during the conventional baseline. Although the baseline check box is designed to minimize gradients, the large gradients between room temperature and the baseline box, as much as 15C, could be expected to exaggerate the effects of any imperfection in the gradient suppression design of the box. It is interesting to note that the mean conventional baseline temperature at Palmyra was 39.9C with a standard deviation of 0.7C while at Christmas Island the mean baseline temperature was 42.2C and the standard deviation was 3.1C.

Following this line of reasoning one may interpret the deviation noted at Palmyra as due to the temperature-frequency insensitivity of the conventional

Pressure (mb)	Christmas Island N=39		Palmyra N=23		Total N=62	
	Average Deviation (°C)	Arithmetic Average Deviation (°C)	Average Deviation (°C)	Arithmetic Average Deviation (°C)	Average Deviation (°C)	Arithmetic Average Deviation (°C)
1000	1.18	1.02	0.58	-0.05	0.96	0.63
800	1.06	0.85	0.54	-0.06	0.87	0.51
600	0.95	0.79	0.51	-0.06	0.79	0.48
400	0.84	0.72	0.44	-0.04	0.69	0.44
200	0.75	0.57	0.35	-0.03	0.60	0.35

$$\text{Average Deviation} = \frac{\sum_{n=1}^{K} |T_P - T_C|_n}{K-1}$$

$$\text{Arithmetic Average Deviation} = \frac{\sum_{n=1}^{K} (T_P - T_C)_n}{K-1}$$

Where T_P is the temperature deduced from the precision baseline

T_C is the temperature deduced from the conventional baseline

Table 1. Comparison of temperature data evaluated using precision and conventional baseline checks.

sonde at high temperatures. However at Christmas Island it would appear that both temperature-frequency insensitivity and the temperature gradient problems were present. Of course some human error was involved in the instrument baseline and data analysis even though the above discussion neglects this point.

In spite of the above comparisonone may still question which answer is more correct, the temperature obtained from the conventional baseline or the one obtained from the precision baseline. We need a test which shows which method gives better, or more realistic, results.

Christmas Island data is representative of the equatorial dry zone, an area which generally experiences very steady weather conditions with remarkably little hour-to-hour or day-to-day variation. For this reason we hypothesized that the baseline procedure which produced the smoother time-sequence of air temperature on a given pressure surface was the better procedure.

The results of these comparisons are shown in Figs. 5 and 6 and table 2. Clearly, the modified baseline procedure produces a smoother time sequence. In addition, it results in approximately 1C larger mean temperature values for all pressure surfaces than does the conventional baseline. This type of analysis was not carriedout for the Palmyra data because Palmyra was in the intertropical convergence zone, a region where one does not expect horizontal and temporal uniformity of temperature.

5. Conclusions

An analysis of Figs. 1 and 3 alone indicates that the resolution of the conventional radiosonde modulator is of questionable adequacy at high temperatures. The relatively simple baseline modulator makes it possible to obtain significantly more accurate temperature data in the tropics with minimal additional cost.

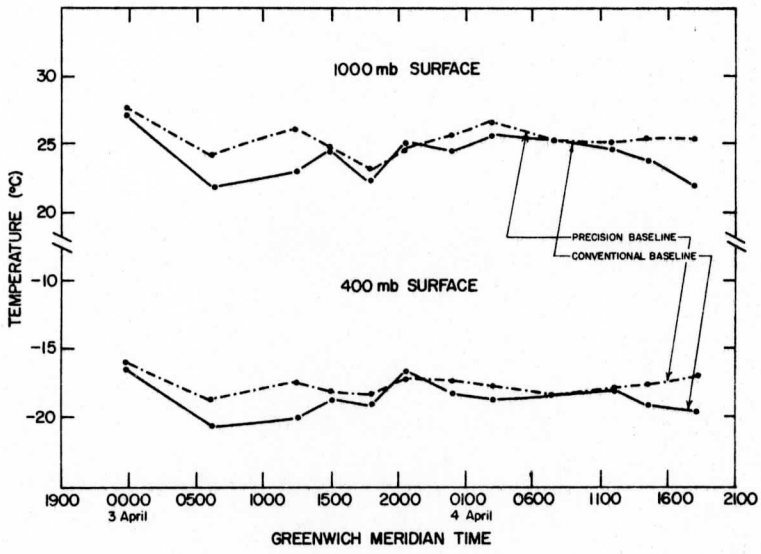

Fig. 5. Comparison of temperature evaluation from precision and conventional baselines for Christmas Island serial ascents, 3, 4 April 1967.

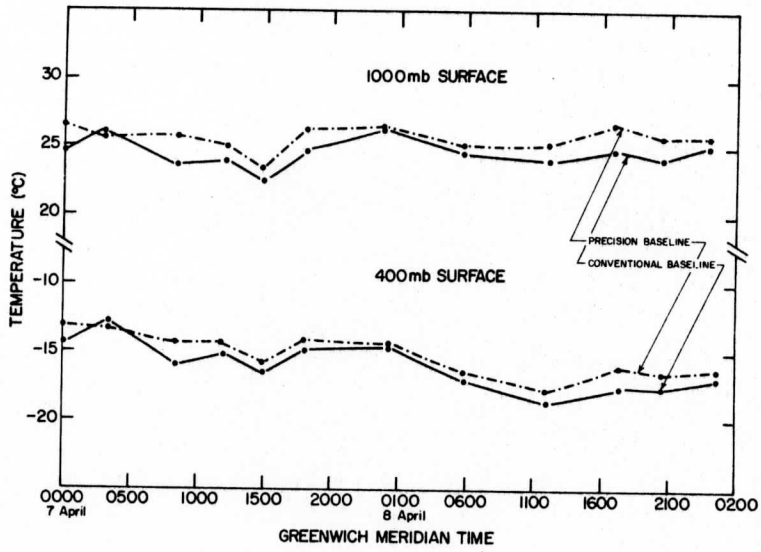

Fig. 6. Comparison of temperature evaluation from precision and conventional baselines for Christmas Island serial ascents, 7, 8 April 1967.

Pressure (mb)	Christmas Island, 3,4 April 1967				Christmas Island, 7,8 April 1967			
	Mean Temperature (°C)		Standard Deviation (°C)		Mean Temperature (°C)		Standard Deviation (°C)	
	Precision	Conventional	Precision	Conventional	Precision	Conventional	Precision	Conventional
1000	25.4	24.2	0.99	1.76	25.7	24.6	0.91	1.03
800	15.6	14.6	0.97	1.46	17.3	16.3	1.86	2.04
600	1.6	1.0	1.35	1.51	3.5	2.5	0.98	0.82
400	-17.7	-18.6	0.65	1.36	-15.1	-15.8	1.47	1.95
200	-53.3	-53.9	1.09	1.33	-53.9	-54.6	0.90	0.89

Table 2. Comparison of Christmas Island serial ascent temperature data evaluated using precision and conventional baseline checks.

The baseline modulator and techniques were developed hastily in order to assure the accuracy of the Line Island upper air data. We do not pretend that these procedures are the ultimate; however, they have shown the need for a review of baseline procedures for conventional radiosondes in tropical environments or whenever high baseline temperatures are encountered. It is beyond the scope of the interest of the authors to further pursue this question; however, it is of extreme importance that the calibration probelms brought out in this study be considered seriously before large investments in future global experiments are made.

Acknowledgements: The development of the precision baseline procedure and the resulting analysis was supported by ESSA Grant WBG 88 at the University of Wisconsin. We would also like to express our thanks to NCAR for inviting us to participate in the Line Island Experiment.

REFERENCES

Hodge, Mary W. and Harmantas, Christos, "Compatibility of United States Radiosonde," "Monthly Weather Review", 93 (4): 253-266, April, 1965.

U. S. Weather Bureau, Manual of Radiosonde Observations (WBAN), Circular P, 7th edition, U. S. Government Printing Office, Washington, D. C., June, 1957.

RADIOMETRIC INFERENCE OF STRATOSPHERIC WATER VAPOR

P. M. Kuhn[1] and S. K. Cox[1]

[1]IQSY Radiation Research Project, ESSA, University of Wisconsin, Madison.

LIST OF SYMBOLS

Δw	Change in mixing ratio (parts per million)
p	Pressure
T	Temperature
0	Subscript denoting surface
θ	Angle (radians)
ν	Wave number (reciprocal centimeters)
τ	Transmissivity
$\bar{I}_b$	Average black body radiance for layer
w	Subscript denoting water vapor
c	Subscript denoting carbon dioxide
o	Subscript denoting ozone
I_b	Black body radiance
F	Downward irradiance (cal cm^{-2} min^{-1})
$F\downarrow_0$	Observed downward irradiance (cal cm^{-2} min^{-1})
$F\downarrow_c$	Calculated downward irradiance
W	Water vapor mixing ratio (ppm)
p_0	Pressure at reference level, 50 mb.
λ	Exponent describing lapse rate of w(p)
$W(p_0)$	Mixing ratio at reference level p_0
$\bar{w}$	Mean water vapor mixing ratio
N	Number of pressure levels at which $F\downarrow_c$ is calculated
du	Increment of optical mass
g	Acceleration due to gravity

ABSTRACT

By varying the amount of water vapor as input to the radiative power transfer equation, assuming a constant carbon dioxide and varying ozone distribution, it is possible to infer stratospheric water vapor from broadband observations of downward irradiance. The procedure is iterative in that downward observed and calculated irradiances, at several levels for each of several radiometric soundings, are brought within the limits of a convergence criterion. This is accomplished by successively reducing an initial over-estimate of the stratospheric mixing ratio, defined by a power law, until the sum of the squared differences of observed and calculated irradiances is minimized. The sum includes all levels of the sounding.

Results for a continental area during winter months indicate that the stratospheric water vapor content from 50 mb upward to 10 mb decreases from approximately 20 to 3 parts per million. For tropical Guam and Canton Island the corresponding magnitudes are larger, decreasing from 21 to 4 ppm. The standard deviation of the mean for all pressure levels is approximately 1.0 ppm. Adding deviation to the values inferred should give an upper bound to the water vapor content. The average mixing ratio for the continental stations between 25 and 10 mb is 5.7 ppm with a standard deviation of the mean of 0.8 ppm. Since the infrared radiative emission and attenuation of aerosols is inseparable from emission and attenuation of the atmospheric gases when measured with a broad response radiometer, these mixing ratio results would be reduced by the presence of aerosols. In view of apparent aerosol contamination we have made no inferences below 50 mb (21 km). The results may be said to be an upper bound to the actual quantity of water vapor, favoring an increasingly dry stratospheric profile.

I. INTRODUCTION

In a recent study, Mastenbrook (1966) presented the results of frost point observations of moisture in the lower stratosphere. His measurements show that the lower stratospheric and upper tropospheric mixing ratio ranges from 2.2-3.2 ppm. A prior publication by Mastenbrook (1965) showed a mixing ratio range of from 1.0-4.0 ppm. The latter work generally agrees with independent spectral measurements and analyses of Houghton et al. (1961) and Calfee and Gates (1966). Murcray et al. (1966), however, indicate a decrease of mixing ratio from approximately 30 through 15 mb with a subsequent increase presumably due to balloon and train contamination. This could also explain Mastenbrook's (1966) results at terminal attitude.

Our purpose is to describe a relatively low-cost radiometric technique for estimating a profile of stratospheric water vapor and to present results of the employment of this technique upwards from 50 mb. Kostyanoy (1965) inferred total water vapor distribution above 100 mb using a similar method on radiometric irradiance data observed over Russia.

In this study over 200 direct observations of downward irradiance are data for a solution of the radiative transfer equation. Downward irradiance calculations are adjusted to reproduce the measured downward irradiance by varying the complete stratospheric water vapor profile. This is accomplished by a least squares method of minimizing the difference between observed and calculated irradiance. When a predetermined irradiance convergence criterion is reached, a unique solution exists.

The basic assumptions for the calculations are:

1) The background for the downward irradiance is zero at 0.1 mb.

2) The carbon dioxide is distributed uniformly at 0.031 per cent by volume.

3) The total optical mass of ozone above 50 mb is 0.212 cm (Craig, 1965). The distribution of ozone is given in Table 1.

4) The presence of optically active aerosols will reduce the inferred water vapor mixing ratios. The average mixing ratio derived may be said to be said to be an average upper bound. Pilipowskyj[2] has shown that radiatively active aerosols may be present as high as 30 mb.

5) The temperature profile from 1.0 to 20.0 mb is taken from Murgatroyd (1957) to fill in high-level temperatures in the downward irradiance calculation. Table 2 gives this profile. It should be noted that a change of $\pm$ 5.0C in the 1.0-mb temperature results in a calculated mixing ratio change of only $\pm$ 0.2 ppm.

The observational requirement is the accumulation of irradiance observations from as high as possible downward through the stratosphere. For this the IQSY radiometersonde network provided the necessary data. The accuracy of these measurements is such that the random error in the evaluation of the mixing ratio is 2.2 ppm.

A computer solution for the convergence of calculated to observed irradiance is, of course, a necessity in view of the large number of calculations required. The procedure is one of least squares, beginning with an overestimate of the input water vapor profile for each atmospheric layer and adjusting the profile downward until the sum of the squared differences of observed and calculated irradiances is reduced to the convergence criterion described in Section 3.

---

[2]Personal communication, S. J. Pilipowskyj, Dept. Meteor., Univ. of Wisconsin.

TABLE 1. Vertical distribution of ozone from 0.1 to 50.0 mb after Craig (1965).

Pressure (mb)	Optical depth (mass) increment (gm cm^{-2})
0.1	0
0.3	0
0.6	0
1.0	0
2.0	0.002
3.0	0.001
5.0	0.005
7.0	0.007
10.0	0.010
15.0	0.020
20.0	0.030
25.0	0.030
30.0	0.030
35.0	0.030
40.0	0.020
45.0	0.015
50.0	0.012

TABLE 2. Temperatures between 0.1 and 20.0 mb after Murgatroyd (1957).

Pressure level (mb)	Summer, 40N (°C)	Winter, 40N (°C)
0.1	-46.0	-30.0
0.4	- 8.0	- 5.0
1.0	+12.0	-13.0
2.0	4.0	-24.0
3.0	- 4.0	-33.0
4.0	-12.0	-39.0
6.0	-24.0	-48.0
8.0	-31.0	-53.0
10.0	-36.0	-56.0
12.0	-40.0	-57.0
16.0	-44.0	-59.0
20.0*	-47.0	-59.0

*Temperatures corresponding to pressures higher than 20.0 mb are observed for the actual ascent.

2. THE OBSERVATIONS OF ATMOSPHERIC IRRADIANCE

To realize a random error of 2.2 ppm in the radiometrically inferred mixing ratio determined by the result of the irradiance convergence criterion, it is necessary that the standard deviation of the radiometersonde not exceed 0.0012 cal cm^{-2} min^{-1}. Analyses of radiometersonde accuracy have appeared in recent meteorological literature. Kuhn and Johnson (1966) show that the standard deviation of a filtered radiometersonde observation due to random error is 0.0012 cal cm^{-2} min^{-1} for a 0.2C radiometersonde sensor temperature error.

Table 3 illustrates a determination of the random error of a derived mixing ratio for two cases with constant mixing ratio profiles. The table is a computer solution of the radiative power transfer equation. The mixing ratio profiles employed are 1.0 and 4.0 ppm. The average irradiance difference for these two calculations is 0.0016 cal cm^{-2} min^{-1}. Assuming an instrumental standard deviation of 0.0012 cal cm^{-2} min^{-1}, the random error in the inferred mixing ratio is 2.2 ppm.

The pressure scaling term for water vapor in both instances is $(p/p_o)^{0.38}$ after Möller and Raschke (1963). Pressure scaling for carbon dioxide is in the form $(p/p_o)^{0.6}$. Elsassers' (1960) water vapor and carbon dioxide flux emissivities were employed. These tables are based on the work of Howard et al. (1955). Temperature scaling in both instances followed the form $(T_o/T)^{0.5}$.

Since the ozone content of the atmosphere above 50 mb can possibly vary by a factor of two, it is necessary to show that such a variation will not obscure the inferred water vapor amounts. Table 4 is an analysis of the contributions of the various gases to the total irradiances at various level. Two calculations were made. The water and carbon dioxide profiles were the same in both calculations.

TABLE 3. Calculated downward irradiance (cal cm^{-2} min^{-1}) for two water vapor profiles.

Pressure (mb)	Temperature (°C)	Mixing ratio* (ppm)	Irradiance*	Mixing ratio** (ppm)	Irradiance**	Δw (ppm)	$F\downarrow_c{}^* - F\downarrow_c{}^{**}$
0.1	-40.0	0.0	0	0.0	0		
0.3	- 2.0	0.0	0.0005	0.0	0.0005		
0.6	7.0	0.0	0.0009	0.0	0.0009		
1.0	4.0	0.0	0.0010	0.0	0.0010		
2.0	-10.0	1.0	0.0071	4.0	0.0092	3.0	0.0021
3.0	-20.0	1.0	0.0085	4.0	0.0102	3.0	0.0017
5.0	-35.0	1.0	0.0010	4.0	0.0115	3.0	0.0014
7.0	-38.0	1.0	0.0111	4.0	0.0123	3.0	0.0012
10.0	-45.0	1.0	0.0129	4.0	0.0140	3.0	0.0011
15.0	-50.0	1.0	0.0149	4.0	0.0159	3.0	0.0010
20.0	-54.0	1.0	0.0165	4.0	0.0175	3.0	0.0010
30.0	-55.2	1.0	0.0199	4.0	0.0211	3.0	0.0012
40.0	-56.5	1.0	0.0221	4.0	0.0243	3.0	0.0021
50.0	-57.6	1.0	0.0236	4.0	0.0265	3.0	0.0029

*First calculation: ozone content is from Table 1; carbon dioxide content is constant at 0.031 per cent by volume; water vapor mixing ratio is given in column 3.

**Second calculation: ozone content is from Table 1; carbon dioxide content is constant at 0.031 per cent by volume; water vapor mixing ratio is given in column 5.

TABLE 4. Calculated downward irradiances (cal cm^{-2} min^{-1}) for two ozone profiles

Pressure (mb)	Temperature (°C)	Total* irradiance	Total** irradiance	H_2O irradiance	CO_2 irradiance	Ozone* irradiance	Ozone** irradiance	$F\downarrow_c^* - F\downarrow_c^{**}$ ozone	Water vapor***
0.1	-40.0	0	0	0.0000	0.0000				
0.3	- 2.0	0.0005	0.0005	0.0000	0.0005				
0.6	7.0	0.0009	0.0009	0.0000	0.0009				
1.0	4.0	0.0010	0.0010	0.0000	0.0010				
2.0	-10.0	0.0092	0.0091	0.0000	0.0024	0.0008	0.0007	0.0001	0.0021
3.0	-20.0	0.0102	0.0102	0.0000	0.0030	0.0007	0.0007	0.0000	0.0017
5.0	-35.0	0.0115	0.0115	0.0050	0.0044	0.0008	0.0007	0.0000	0.0014
7.0	-38.0	0.0123	0.0122	0.0054	0.0056	0.0007	0.0006	0.0000	0.0012
10.0	-45.0	0.0140	0.0138	0.0056	0.0072	0.0008	0.0006	0.0002	0.0011
15.0	-50.0	0.0159	0.0154	0.0055	0.0089	0.0013	0.0008	0.0005	0.0010
20.0	-54.0	0.0175	0.0167	0.0054	0.0101	0.0018	0.0010	0.0008	0.0010
30.0	-55.2	0.0211	0.0202	0.0056	0.0126	0.0025	0.0016	0.0009	0.0012
40.0	-56.5	0.0243	0.0233	0.0067	0.0143	0.0030	0.0020	0.0010	0.0021
50.0	-57.6	0.0265	0.0256	0.0073	0.0155	0.0033	0.0024	0.0009	0.0029

*First calculation: ozone content from Table 1; water vapor mixing ratio constant at 4.0 ppm for pressure $\geq$ 2.0 mb; carbon dioxide content is constant at 0.031 per cent by volume.

**Second calculation: ozone contant one-half that of Table 1; water vapor mixing ratio constant at 4.0 ppm for pressure $\geq$ 2.0 mb.

***$F\downarrow_c^{**} - F\downarrow_c^{*}$ from Table 3.

The ozone profile for the first calculation was halved at each level. The difference in the radiative contribution of the ozone from the first to the second calculation is given in the column, "$F\downarrow_c^{*}$--$F\downarrow_c^{**}$, ozone". For comparison, the last column of Table 3 lists the difference in the radiative contribution of water vapor in two calculations having constant mixing ratios of 4.0 and 1.0 ppm, respectively. From the last two columns of Table 4, it is apparent that the effects of halving the ozone content are approximately a factor of two less than those radiative effects of a water vapor reduction of 3.0 ppm.

Approximately eighty IQSY radiometric ascents at Guam, Marianas Islands, Canton Island, Green Bay, Wisc., and Washington, D. C., were used in this analysis. All of these ascents exceeded terminal elevations of 15mb and averaged 6 $\pm$ 2 mb at highest altitude. The observations were taken between October 1964 and March 1965.

3. CALCULATED RADIANT POWER AND INFERRED WATER VAPOR

Since the irradiance observed by a flat plate radiometer ascending in the atmosphere is related to the atmospheric temperature, pressure, water vapor, carbon dioxide, ozone, and aerosol profiles, the radiative power transfer work (Wark and Fleming, 1966; Elsasser, 1960) uniquely expresses this relationship only in the absence of aerosols. For a plane parallel atmosphere, containing no scatterers, and in local thermodynamic equilibrium, the radiative transfer equation, expressed in terms of radiance, is given by

$$I(\theta) = \int_{\nu_1}^{\nu_2}\int_{1}^{\tau(P_0,\nu)} \bar{I}_b\left(\nu, T(P)\right) d\tau(\nu,P)_w d\nu - \int_{\nu_1}^{\nu_2}\int_{1}^{\tau(P_0,\nu)} \bar{I}_b\left(\nu, T(P)\right) d\tau(\nu,P)_c d\nu$$

$$- \int_{\nu_1}^{\nu_2}\int_{1}^{\tau(P_0,\nu)} \bar{I}_b\left(\nu, T(P)\right) d\tau(\nu,P)_0 d\nu + I_b(\nu,P_0)\tau(\nu,P_0)_c \tau(\nu,P_0)_0 \qquad (1)$$

Irradiance, measured by the radiometersonde, is related directly to radiance, Eq. (1), by the expression

$$F = 2\pi \int_0^{\theta_1} \bar{I}_b(\theta) \cos\theta \sin\theta d\theta \qquad (2)$$

where the limit θ_1 is $\pi/2$ radians.

Thus, Eq. (2) represents a three-fold integration

1) over all angles θ,

2) over all frequencies of radiation ν, and

3) over all transmissivities of the absorbing gas τ.

Elsasser (1960) has shown that replacing the monochromatic radiance $I_b(\nu)$ or spectral radiance I_b by the monochromatic irradiance $F_b(\nu)$ or by the spectral irradiance F_b does not change the basic transfer formalism of Eq. (1). Combining Eqs. (1) and (2) and considering only hemispheric downward irradiance, integrated over all wavelengths (fourth term on right hand side in Eq. (1) is zero), the downward irradiance is given by

$$F\downarrow_c = -\int_1^{\tau F(P_0)_w} \bar{F}_b\left(T(P)\right) d\tau F(P)_w - \int_1^{\tau F(P_0)_c} \bar{F}_b\left(T(P)\right) d\tau F(P)_c$$

$$- \int_1^{\tau F(P_0)_0} \bar{F}_b\left(T(P)\right) d\tau F(P_0) \qquad (3)$$

where $\bar{F}_b$ is the black body irradiance equal to $\pi\bar{I}_b$ and τ_F is the irradiance transmissivity.

Knowing the irradiance, and temperature profile from 0.1 mb down to approximately 50 mb, we can solve the transfer equation for all levels, assuming a water vapor profile w(P). The data for the computer program are pressure, mean temperature for each layer, ozone concentration, carbon dioxide concentration, and the assumed water vapor mixing ratio w(p), for each level.

After observing that level-by-level computations of water vapor agreed well with a power function representation of the vapor profile, further water vapor deductions were made assuming a power function representation given by

$$w(p) = w(p_o)\left(\frac{p}{p_o}\right)^{\lambda} \tag{4}$$

This function was suggested by Smith (1966). It should be noted that the power function approximation can describe an increase in mixing ratio with decreasing pressure when lambda is negative. This possibility was considered; however, it was not possible to make the observed and calculated irradiance values approach agreement using reasonable values for $w(p_o)$ when lambda was negative. Typically, λ ranged between 0.0 and 1.0, and $w(p_o)$ between 40.0 and 5.0 ppm. In addition, the calculation of the downward irradiance requires that the water vapor contribution be zero at that pressure where carbon dioxide emission accounts for the entire downward irradiance. The changing of an entire water vapor profile by the power function approximation of Eq. (4) imposes a stabilizing constraint on the solution of Eq. (1) that is not possible in a level-by-level iteration.

Moreover, the solution of (1) for water vapor is more efficient when (4) is employed. Initially, overestimation of the profile of $\bar{w}$ (gm kg^{-1}) is made by employing the maximum $w(p_o)$ and minimum λ. The profile is then successively reduced until the quanity $\sum (F\downarrow_o - F\downarrow_c)^2$ reaches the predetermined convergence criterion, $N(0.0012)^2$.

The pressure and temperature scaled precipitable centimeters of water vapor and mixing ratio are output for each computed level when convergence occurs. The mean mixing ratio between two successive pressure levels is given by the expression

$$\bar{w} = du\left(\frac{g}{dp}\right)\left(\frac{p_o}{p}\right)^{0.38}\left(\frac{T}{T_o}\right)^{0.5} \qquad (5)$$

4. RESULTS

Figs. 1 through 5 are typical profiles of observed irradiance and inferred water vapor mixing ratios in parts per million. The errors in pressure and irradiance are indicated by bars on the plotted points for observed downward irradiance at Green Bay in Fig. 1. This figure also illustrates the least square fitted curve of irradiance for the plotted data points. Such a curve was fitted to each of the 210 ascents employed in the study. However, convergence of calculated-to-actual observed data was accomplished at the 7-, 10-, 15-, 20-, 25-, 30-, 35-, and 50-mb levels. An attempt has been made to clearly compress as much data as possible into each figure and yet retain a measure of simplicity.

A feature of some of the observed irradiance values is the tendency for the

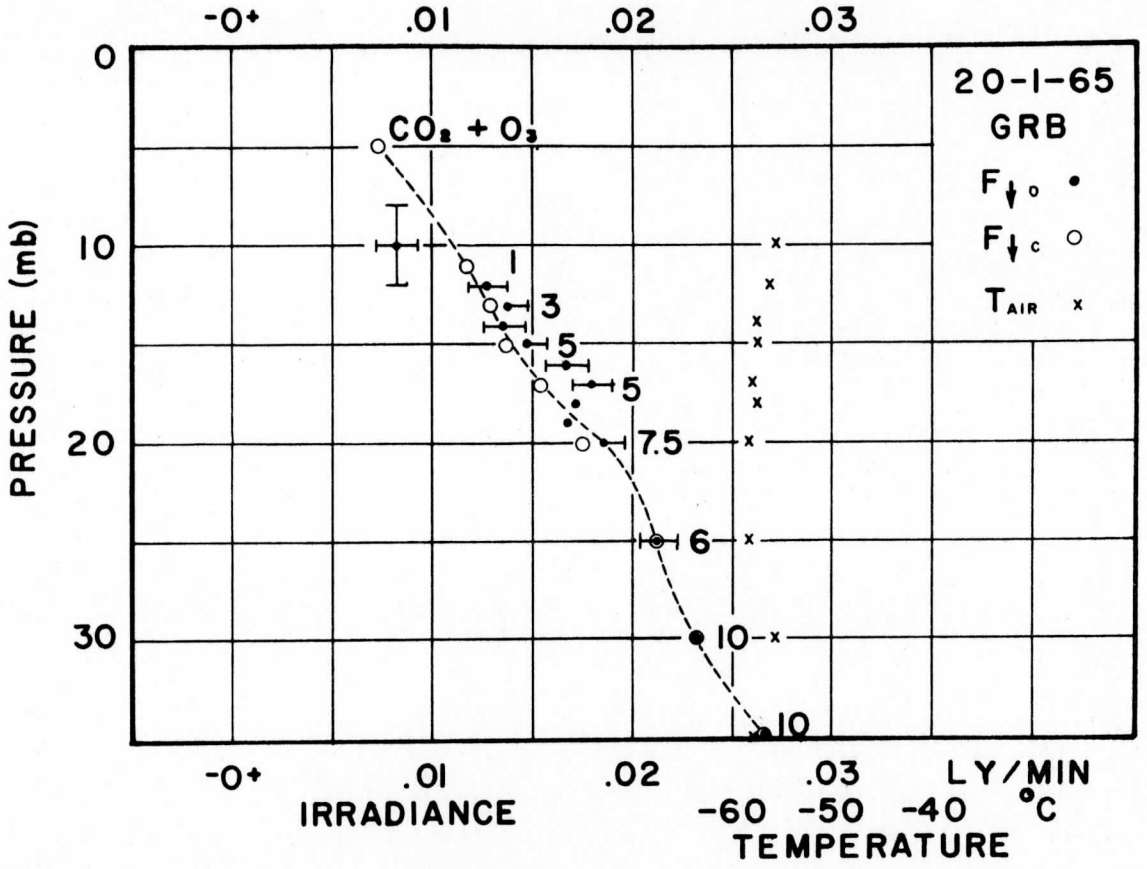

FIG. 1. Profile of observed $F\downarrow_o$ and calculated $F\downarrow_c$ downward irradiance and air temperature for Green Bay, Wisc. (GRB), 20 January 1965. Horizontal error bars indicate one standard deviation of observed irradiance due to random instrument error. Vertical error bar indicates radiosonde pressure error. Numbers adjacent to calculated irradiance in this and succeeding figures indicate mixing ratio of water vapor in parts per million required for minimizing calculated-observed irradiance difference.

magnitude of the highest one or two irradiance observations, immediately prior to balloon burst, to fall below that which carbon dioxide alone contributes. Pressure scaling for the carbon dioxide optical mass is critical at such levels. There is also the possibility of a systematic error in the instrument at such high altitudes due to a loss of convective temperature coupling of the environment to the polyethylene convection shields. This could cause a small conduction error in the solution of the radiometer equation. However, at pressures greater than 10 mb the convergence criterion of observed and calculated downward radiant power is easily achieved.

The water vapor results illustrated in these figures demonstrate the possibilities of the use of irradiance observations to infer stratospheric water vapor. The examples were not chosen to typify the average profiles listed in Table 5. It should be recalled that we are using the water vapor and carbon dioxide transmissivities of Howard et al. (1955) converted to slab emissivities for the transfer computations and that the maximum resolution of the radiometrically inferred mixing ratios, due to random errors in the irradiance observations, is 2.2 ppm.

Figs. 1 and 2 are continental profiles of water vapor displaying a decrease in water vapor with height from 35 through 5 mb (pressure error is $\pm$ 2.0 mb). In Fig. 2, the mixing ratio is constant from 35 through 20 mb. Above this level the decrease in mixing ratio with height, common to the majority of our ascents coupled with the steady decline in the optical mass of carbon dioxide, is reflected in the decrease in the observed and calculated irradiance. This decrease occurs in the presence of a slight increase in temperature with height. The rapidly decreasing concentration of radiant power absorbers and emitters and the

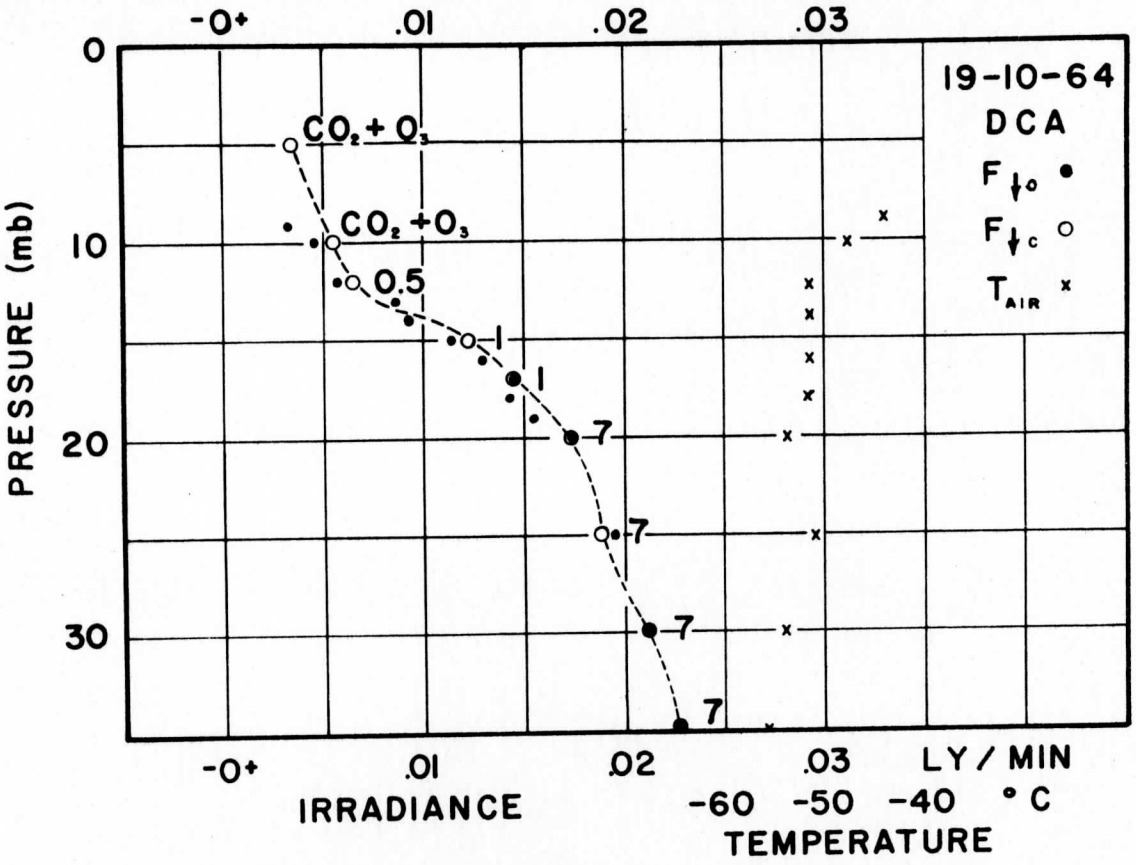

FIG. 2. Profiles of observed $F\downarrow_o$ and calculated $F\downarrow_c$ downward irradiance and air temperature for Washington, D. C. (DCA), 19 October 1964.

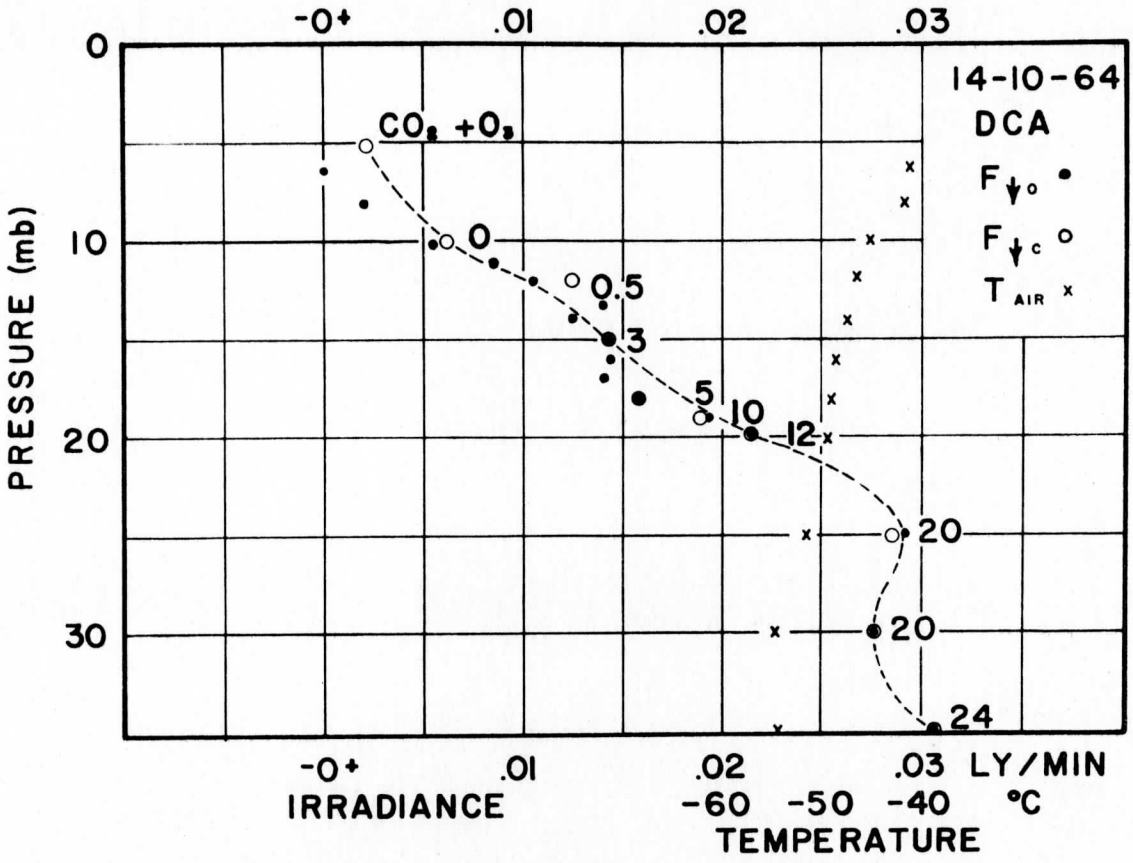

FIG. 3. Profiles of observed $F_{\downarrow o}$ and calculated $F_{\downarrow c}$ downward irradiance and air temperature for Washington, D. C. (DCA), 14 October 1964.

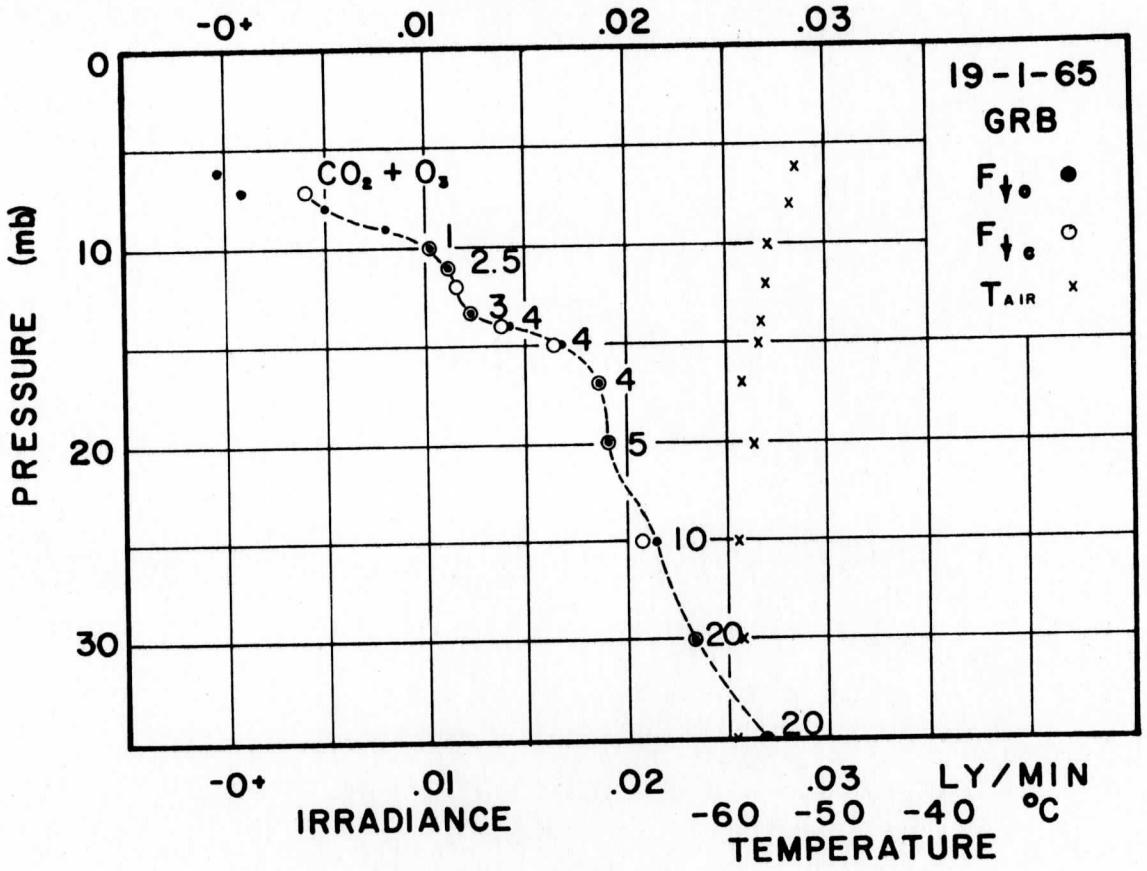

FIG. 4. Profiles of observed $F\downarrow_o$ and calculated $F\downarrow_c$ downward irradiance and air temperature for Green Bay, Wisc. (GRB), 19 January 1965.

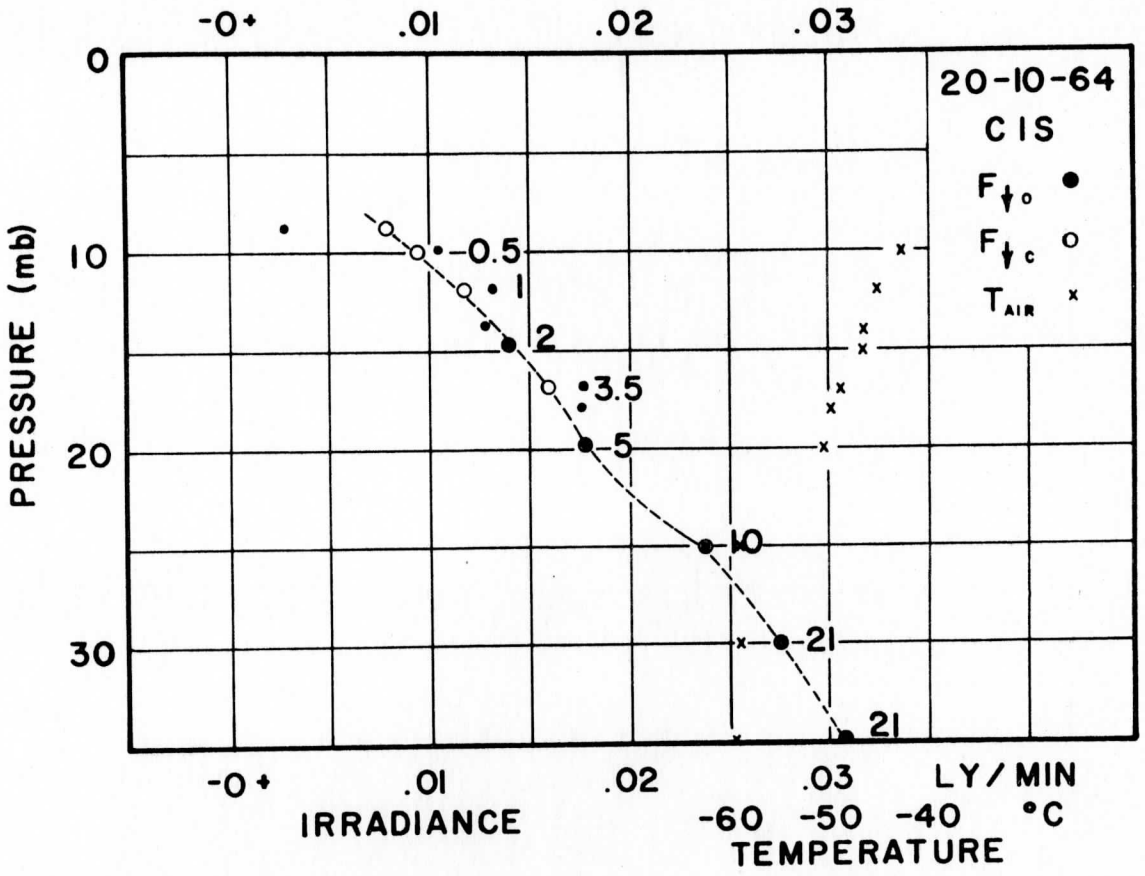

FIG.5. Profiles of observed $F\downarrow_o$ and calculated $F\downarrow_c$ downward irradiance and air temperature for Canton Island (CIS), 20 October 1965.

zero background radiation counteract the temperature increase. Recent general concern over contamination during ascent of frost point moisture measuring equipment indicates a possible modification of the concept of rapidly increasing mixing ratio above 50 mb.

Figs. 3 and 4 illustrate "wetter" continental mixing ratio profiles that were observed in 25 per cent of the observations. These results show a decrease in mixing ratio with height.

Fig. 5, for Canton Island, demonstrates a typical stratospheric inferred water vapor profile for the tropics above 35 mb. There is no tendency toward a constant mixing ratio. The average sounding in the tropics for this study was considerably more moist than the continental mean sounding.

The first five columns of Table 5 summarize the mean mixing ratio in parts per million, and the standard deviation of the mean for the various station groups and pressure levels. Groupings were arranged to achieve a statistically significant quantity of data and were carried down to 50 mb. The random error of 2.2 ppm in the inferred mixing ratio does not limit estimation of mixing ratio to values larger than 2.2 ppm. It is rather a 68 per cent confidence limit.

Several points are evident from this summary. Primarily, the radiometrically inferred water vapor profile decreases with height. Except for the 10-mb level, the standard deviation of the mean remains approximately constant with height. There is a significant difference in the continental and tropical means for the levels included. Possibly, tropical thermal injection of moisture into the stratosphere results in the mean oceanic soundings displaying more water vapor than the mean continental soundings.

The remaining columns of Table 5 list, for comparison, the measured water

TABLE 5. Statistical summary and comparison of inferred water vapor (ppm)

Station group	Pressure (mb)	Number of observations	Average mixing ratio	Standard deviation of mean	Masten-brook mixing ratio	Murcray et al. mixing ratio	Calfee and Gates mixing ratio	Zander mixing ratio
Washington	10	37	2.7	0.3		12.0	2.8	10.0
Madison	15	37	4.9	0.7	3.2	4.9	2.8	10.0
Green Bay	20	37	6.8	1.0	2.7	6.8	2.8	10.0
	25	35*	8.3	1.2	2.6	8.4	2.8	10.0
	50	35	20.1	1.5	2.3	3.5	2.8	
Guam, Canton Is.	10	33	4.1	0.1	2.2			
	15	33	12.8	1.3	2.2			
	20	33	19.0	1.3	2.2			
	25	32*	21.0	1.1	2.2			
	50	32	21.2	1.5	2.2			
Continental average (10,15,20,25 mb)		146	5.6	0.5				
Tropical average (10,15,20,25 mb)		131	14.2	0.9				

*Data missing for some observations.

vapor mixing ratios for corresponding pressure levels by Mastenbrook (1966), Murcray et al. (1966), and Zander (1966), and the calculations of Calfee and Gates (1966). From 25 through 15 mb, Murcray's data agree quite closely with the continental data of this study. Calfee and Gates show less moisture from 25 through 15 mb than the present study and that of Mastenbrook (1966).

The optical depths for continental stations from 50 through 15 mb reported by this study, by Mastenbrook and by Gates, are approximately 1.2, 1.7, and 1.0 μ, respectively. Mastenbrook's (1966) mixing ratio data at pressures equal to and lower than 20 mb may indicate contamination by moisture from the balloon train.

Murcray's results give approximately the same optical depth for the 50-10 mb layer as this study while Zander's results indicate a total optical depth, for the layer discussed, of 4.1 μ.

Balloon-borne radiometer measurements made by Williamson (1964) in the spectral region 5.5-7.0 μ above the tropopause show an essentially constant mixing ratio of approximately 3.0 ppm. This corresponds to a total optical depth in the layer 50 through 10 mb of approximately 1.2 μ. Kostyanoy's (1965) radiometrically inferred water vapor optical depth above 100 mb for 16 radiation sonde ascents over western USSR averaged 35.0 μ. Assuming a constant mixing ratio with height, his results would indicate 14.0 μ in the 50-10 mb layer.

The radiometrically inferred water vapor profile of this research from 50 through 100 mb gives values up to 40 ppm and may indicate broad band aerosol radiative "contamination" at pressures greater than 35-50 mb. These values average higher than most direct measurements for the 50 through 100 mb layer and are not reported on in detail. The increase in deduced water vapor below

the 35-mb level suggests that a radiatively effective upper limit for atmospheric aerosols may exist for these radiation soundings at approximately 35 mb.

Fig. 6, after the technique of Gutnick (1961), compares recent measurements and calculations of stratospheric water vapor profiles between 50 and 10 mb by a number of researchers. Mastenbrook's (1965) data, showing constant mixing ratio with height, curve M_1, has been included.

5. CONCLUSIONS

Water vapor is the only variable in the radiative power transfer calculation when the distribution of the other gases is known and the temperature profile is known. By varying the amount of water vapor input to the radiative transfer calculation we can successively adjust the water vapor profile to obtain convergence of water vapor calculations with direct observations to a preset limit. This convergence criterion is determined by the random error of the radiometer. Knowing this error, we then infer water vapor quantities from direct observations of irradiance.

Our results, for the winter months, for tropical and mid-latitude continental areas in 1964 and 1965, indicate that the stratospheric water vapor content above 30 mb for continental regions averages 5.6 ppm with a standard deviation of the mean of 0.5 ppm. For the tropics these quantities are 14.2 and 0.9 ppm, respectively. Radiative aerosol "contamination" is a problem below 35 mb as this radiative effect is inseparable from that of water vapor. The radiometrically inferred water vapor mixing ratios do not display a tendency toward a constant mixing ratio with height but rather show a decrease in mixing ratio with height above 50 mb.

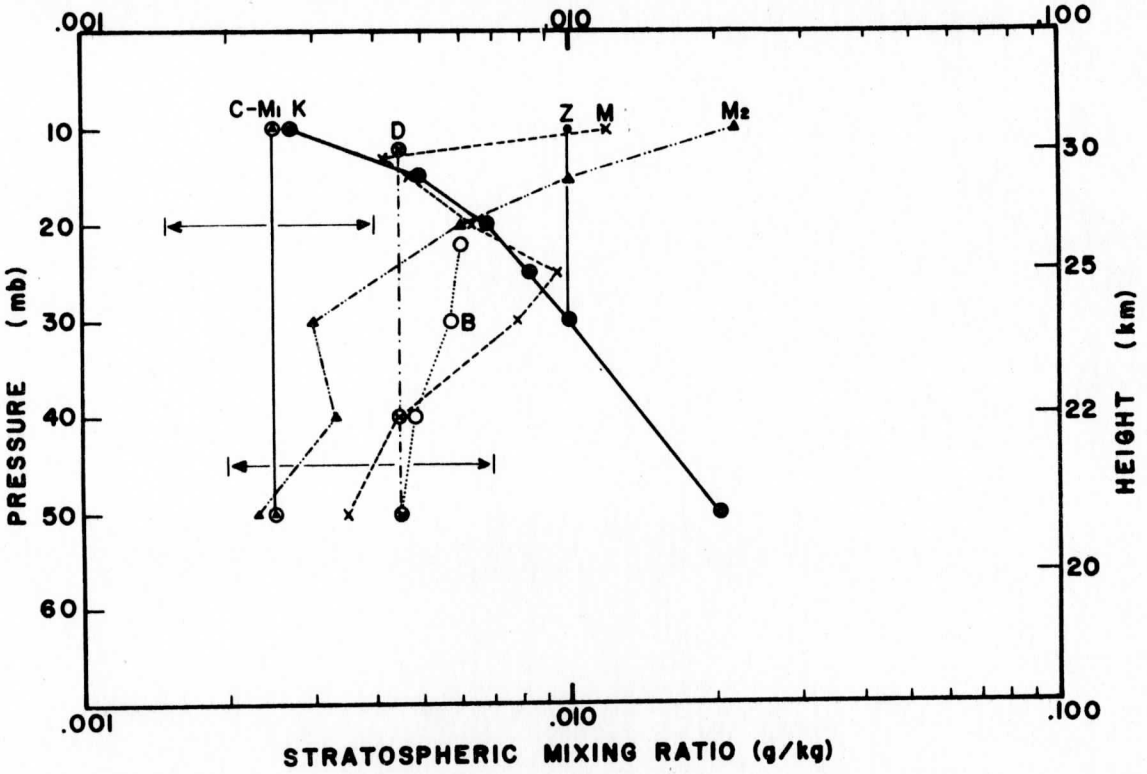

FIG. 6. Stratospheric water vapor profiles: C, Calfee and Gates (1966); M_1, Mastenbrook (1965); K, Kuhn and Cox (present study); D, Dobson et al. (1962); Z, Zander (1966); M, Murcray et al. (1966); M_2, Mastenbrook (1966); B, Ballinger et al. (1965).

REFERENCES

Ballinger, J. G., L. E. Koehler, M. P. Fricke and R. D. Murphy, 1965: Towards improved measurements of stratospheric humidity with balloon-borne frost point hygrometers. Proc. 1964 AFCRL Scientific Balloon Symposium, AFCRL-65-486, A. F. Surveys Geophys., No. 167, 231-256.

Calfee, R. F., and D. M. Gates, 1966: Calculated slant-path absorption and distribution of atmospheric water vapor. Appl. Optics, 5, 287-292.

Craig, R. A., 1965: Physics of the Upper Atmosphere, New York. Pergamon Press, 365 pp.

Dobson, G. M. B., A. W. Brewer and J. T. Houghton, 1962: The humidity of the stratosphere. J. Geophys. Res., 67, 902-903.

Elsasser, W. M., 1960: Atmospheric radiation tables, Meteor. Monogr., 4, No. 23, 43 pp.

Gutnick, M., 1961: How dry is the sky? J. Geophys. Res., 66, 2867-2871.

Houghton, J. T., N. D. P. Hughes, T. S. Moss and J. S. Seeley, 1961: An atlas of the infrared solar spectrum from 1 to 6.5μ observed from a high-altitude aircraft. Phil. Trans. Roy. Soc., London, A254, 47 pp.

Howard, J. N., D. L. Burch and D. Williams, 1955: Near-infrared transmission through synthetic atmospheres. Geophys. Res. papers, No. 40, Air Force Cambridge Research Laboratories, 127 pp.

Kostyanoy, G. N., 1965: On the change of the longwave radiation field in the atmosphere during winter. Isv., Atmos, and Oceanic Phys., Ser. 1, 823-832.

Kuhn, P. M., and D. R. Johnson, 1966: Improved radiometersonde observations of atmospheric infrared irradiance. J. Geophys Res., 71, 367-373.

Mastenbrook, H. J., 1965: The vertical distribution of water vapor over Kwajalein Atoll, Marshall Islands. Naval Research Lab. Report 6367, 11 pp.

_____, 1966: Water vapor observations at low, middle and high latitudes during 1964 and 1965. Naval Research Lab. Report 6447, 21 pp.

Möller, F., and E. Raschke, 1963: Evaluation of Tiros III radiation data. Interim Report No. 1, NASA Grant NsG-305, Ludwig-Maximilians-Universitat-Meteorologisches Institut, München, Germany, 84 pp.

Murcray, D. G., F. H. Murcray and W. J. Williams 1966: Further data concerning the distribution of water vapor in the stratosphere. Quart. J. R. Meteor. Soc., 92, 159-161.

Murgatroyd, R. J., 1957: Wind and temperatures between 20 km and 100 km-a review. Quart. J. R. Meteor. Soc., 83, 417-421.

Smith, W. L., 1966: Satellite inferred atmospheric water vapor and temperature profiles. Ph.D. thesis, University of Wisconsin, 142 pp.

Wark, D. Q., and H. E. Fleming, 1966: Indirect measurements of atmospheric temperature profiles from satellites. Mon. Wea. Rev., 94, 351-362.

Williamson, E. J., 1964: Balloon measurements of emission from the 6.3 micron water vapor band. Mem. Soc. Roy. Sci. Liege, 9, 327-335.

Zander, R., 1966: Moisture contamination at altitude by balloon and associated equipment. J. Geophys. Res., 71, 3775-3778.